

Review

Applications of Spent Lithium Battery Electrode Materials in Catalytic Decontamination: A Review

Pu Wang¹, Yaoguang Guo^{1,*} , Jie Guan¹ and Zhaohui Wang^{2,3,4,*}

¹ Shanghai Collaborative Innovation Centre for WEEE Recycling, School of Resources and Environmental Engineering, Shanghai Polytechnic University, Shanghai 201209, China

² Shanghai Key Lab for Urban Ecological Processes and Eco-Restoration, School of Ecological and Environmental Sciences, East China Normal University, Shanghai 200241, China

³ Technology Innovation Center for Land Spatial Eco-Restoration in Metropolitan Area, Ministry of Natural Resources, 3663 N. Zhongshan Road, Shanghai 200062, China

⁴ Shanghai Engineering Research Center of Biotransformation of Organic Solid Waste, Shanghai 200241, China

* Correspondence: ygguo@sspu.edu.cn (Y.G.); zhwang@des.ecnu.edu.cn (Z.W.)

Abstract: For a large amount of spent lithium battery electrode materials (SLBEMs), direct recycling by traditional hydrometallurgy or pyrometallurgy technologies suffers from high cost and low efficiency and even serious secondary pollution. Therefore, aiming to maximize the benefits of both environmental protection and e-waste resource recovery, the applications of SLBEM containing redox-active transition metals (e.g., Ni, Co, Mn, and Fe) for catalytic decontamination before disposal and recycling has attracted extensive attention. More importantly, the positive effects of innate structural advantages (defects, oxygen vacancies, and metal vacancies) in SLBEMs on catalytic decontamination have gradually been unveiled. This review summarizes the pretreatment and utilization methods to achieve excellent catalytic performance of SLBEMs, the key factors (pH, reaction temperature, coexisting anions, and catalyst dosage) affecting the catalytic activity of SLBEM, the potential application and the outstanding characteristics (detection, reinforcement approaches, and effects of innate structural advantages) of SLBEMs in pollution treatment, and possible reaction mechanisms. In addition, this review proposes the possible problems of SLBEMs in practical decontamination and the future outlook, which can help to provide a broader reference for researchers to better promote the implementation of “treating waste to waste” strategy.

Keywords: spent lithium battery; catalytic oxidation; pretreatment; reaction mechanism



Citation: Wang, P.; Guo, Y.; Guan, J.; Wang, Z. Applications of Spent Lithium Battery Electrode Materials in Catalytic Decontamination: A Review. *Catalysts* **2023**, *13*, 189. <https://doi.org/10.3390/catal13010189>

Academic Editor: Wenhui Wang

Received: 28 November 2022

Revised: 6 January 2023

Accepted: 11 January 2023

Published: 13 January 2023



Copyright: © 2023 by the authors. Licensee MDPI, Basel, Switzerland. This article is an open access article distributed under the terms and conditions of the Creative Commons Attribution (CC BY) license (<https://creativecommons.org/licenses/by/4.0/>).

1. Introduction

To further achieve the environmental goal of sustainable development, electric vehicles (EVs) have been developed rapidly. Currently, the EVs are approximately 7.2 million units, which are predicted to further increase to 245 million units in 2030 [1]. The lifespan of lithium batteries (LIBs) used in EVs is usually 3–10 years. Statistically, the number of end-of-life EVs will reach 6.76 million in 2035, directly leading to the explosion of spent LIBs [2]. High quantities of spent LIBs may pose a significant safety threat for both the environment and human health. The recycling of spent LIBs is important in terms of economics and environmental sustainability, pursuing maximum economic benefits while reducing environmental pollution. However, the recycling of SLBEMs by conventional recycling methods (e.g., hydrometallurgical and pyrometallurgical) has temporary difficulties at the current stage. Large amounts of equipment costs, energy costs, and toxic gases are incurred in pyrometallurgical recovery processes. The recovered products are often lower-purity mixed-metal oxides that require further processing and refining [3]. Compared to pyrometallurgy, the operational steps of hydrometallurgy are more complex. Various acid or alkaline solutions are used in the pursuit of high-purity products. Their subsequent treatment and leakage can significantly reduce the economic benefits of LIBs recovery,

and may even pose safety hazards to human health and the environment [4]. From the perspective of environmental protection and maximum utilization of e-waste resources, greener and more economical recycling methods for SLBEMs deserve further investigation.

In recent years, increasing concentrations of various organic pollutants have been identified (volatile organic pollutants, pharmaceuticals, pesticides, azo dyes, etc.), which may be harmful to human health and environmental safety [5–8]. With the low efficiency in traditional water treatment methods (e.g., biodegradation, physical filtration, and UV disinfection) for the removal of persistent organic pollutants, advanced oxidation technologies (AOPs) with high efficiency, easy operation, and low cost have been widely considered and applied [9–12]. Transition metals (e.g., Ni, Co, Mn, Al, and Fe) are known to induce Fenton-like reactions, photocatalytic reactions, and thermocatalytic reactions for the purification of organic pollutants in water and air [13–15]. Typically, spent LIBs are mainly composed of a cathode material, anode material, electrolyte, separator, and steel case, in which the separator and electrolyte undertake the functions of separating the cathode and anode material and medium in the charging and discharging process, respectively (Figure 1a). It is noteworthy that SLBEMs have inherent advantages as catalysts in catalytic decontamination. On the one hand, the cathode material contains abundant transition metals. Lithium nickel cobalt aluminum acid (NCA), lithium cobaltate (LCO), lithium nickel cobalt manganese (NCM), and lithium iron phosphate (LFP) batteries contain 31 wt%, 41 wt%, 26 wt%, and 25 wt% of cathode materials, respectively [16,17]. It is expected that abundant transition metals on electrode material surfaces may facilitate the catalytic reaction in pollutants decontamination by providing more reactive active sites and enhancing the redox capacity of catalysts.

On the other hand, the charge and discharge cycles require lithium ions (red balls) to successfully complete the embedding and de-embedding cycles between the cathode and anode materials (Figure 1b). When lithium ions cannot be de-embedded from the anode materials, the performance of LIBs decreases with the loss of more lithium ions. Collapses, distortions, or cracks may be formed in the crystal structure of the cathode materials. Vacancies and defects may be created on the cathode material surface during this process, which greatly facilitates the promotion of catalytic reactions on the LIBs surface by improving the electron transfer capacity and oxygen adsorption capacity [18,19]. Moreover, carbon resources (up to 7 wt%) in anode materials can be used as high-performance catalyst substrates [20,21]. The properties of carbon materials with high electrical conductivity and specific surface area are beneficial to improve the catalytic performance of catalysts. Moura et al. initially synthesized the nanostructure LIBs-based photocatalyst (CoFe_2O_4) using the co-precipitation method to establish a photo-Fenton system for MB removal [22]. More than 85% MB was degraded within 400 min. The feasibility and good potency of the combination of spent LIBs electrode materials and AOPs for organic pollutant removal were demonstrated. Up to now, various LIBs-based catalysts have been applied in the catalytic reactions. For example, Xin et al. adopted lithium manganate (LMO) to prepare a high-performance manganese-based thermal catalyst (LMO-MnO_2). Toluene was completely removed at low temperatures ($T_{90} = 224\text{ }^\circ\text{C}$) [23]. In addition, spent LIBs have inherent advantages in catalytic decontamination. Wang et al. found that structural defects and oxygen vacancies (O_v) created on the LFP surface due to lithium-ion loss during charging and discharging were more favorable for catalytic reactions, and the removal rates of bisphenol S (BPS) and rhodamine B (RhB) in the LFP/S(IV) system were 75% and 100% within 45 min, respectively [24]. Similarly, Yue et al. used the hydrothermal method to synthesize a photocatalyst (NaFeS_2), which achieved 98% degradation of methylene blue (MB) in 20 min under visible light [25]. Therefore, the combination of spent LIBs and AOPs for the removal of organic pollutants holds good development prospects.

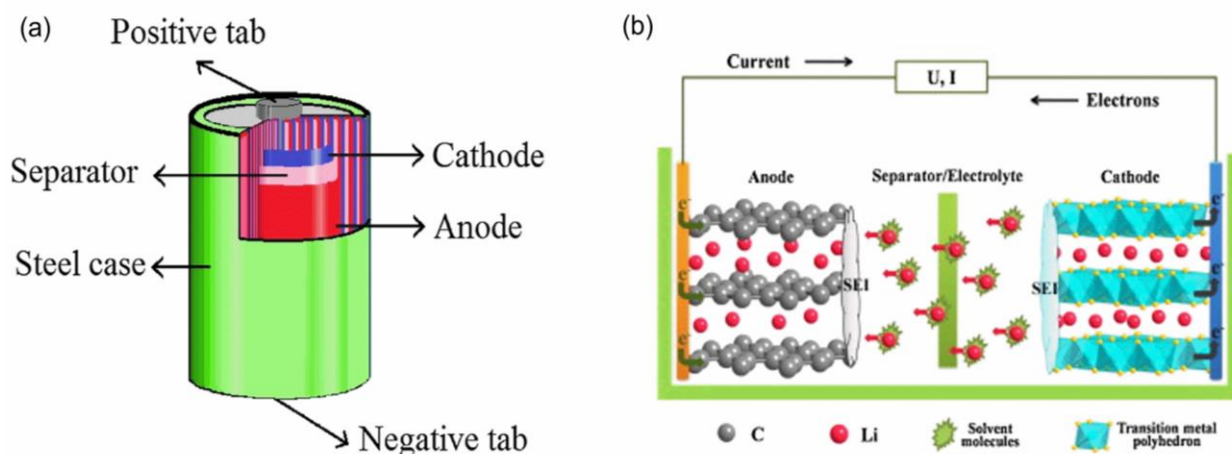


Figure 1. (a) Components and (b) working principles of LIBs. Reprinted with permission from refs. [26,27].

Currently, the review on spent LIBs recovery focuses on the pretreatment of LIBs (e.g., discharging, pre-sorting, and separating), recovery of metal resources (e.g., hydrometallurgical and pyrometallurgical methods), or synthesis of other functional materials for diverse applications [3,28–33]. Other reviews have given a broad introduction to the environmental issues of lithium-ion batteries or different applications (e.g., photocatalysis, thermal catalysis, and transition metal catalysis) [32–37]. Possible problems in the current development of LIBs-based catalysts, more in-depth discussion on the catalytic mechanism, and key influencing factors for catalytic activity are not being systematically discussed from pretreatment and catalyst synthesis to practical application of catalytic decontamination. In our review, the combination of spent LIBs and AOPs in catalytic decontamination is clearly summarized and analyzed based on previous reports. First, this review provides an overview of treatment methods about spent LIBs synthesized as catalysts, such as pretreatment, dissolution in acid/alkaline solutions, and different synthesis methods, and the effect of treatment methods on catalytic activity is also discussed. Then, the key factors influencing catalytic activity, the main issues in the practical decontamination process, and the reaction mechanisms are proposed. Finally, possible problems and future trends in catalytic decontamination are discussed.

2. Spent LIBs for Catalysts Preparation

2.1. LIBs Components

LIBs are usually divided into four parts (cathode, anode, separator, and electrolyte) [38,39]. The cathode material consists of active metal oxides containing transition metals (e.g., Ni, Co, Mn, Fe, and Al), binder, carbon black (conductive carbon), and aluminum foil (Figure 2a). The anode material mainly consists of carbon material and copper foil (Figure 2b). The binder serves to fix active metal oxides and carbon material on aluminum or copper foil, respectively. The average proportion of each component in LIBs is shown in Figure 2c. Active metal oxides (31%) occupy the highest percentage in LIBs. More details of metal oxides are shown in Figure 2d. The stable arrangement of transition metals in diverse crystal structures and the large distribution on material surfaces offer great possibilities for the catalytic processes on catalyst surfaces and a good stability of LIBs-based catalysts.

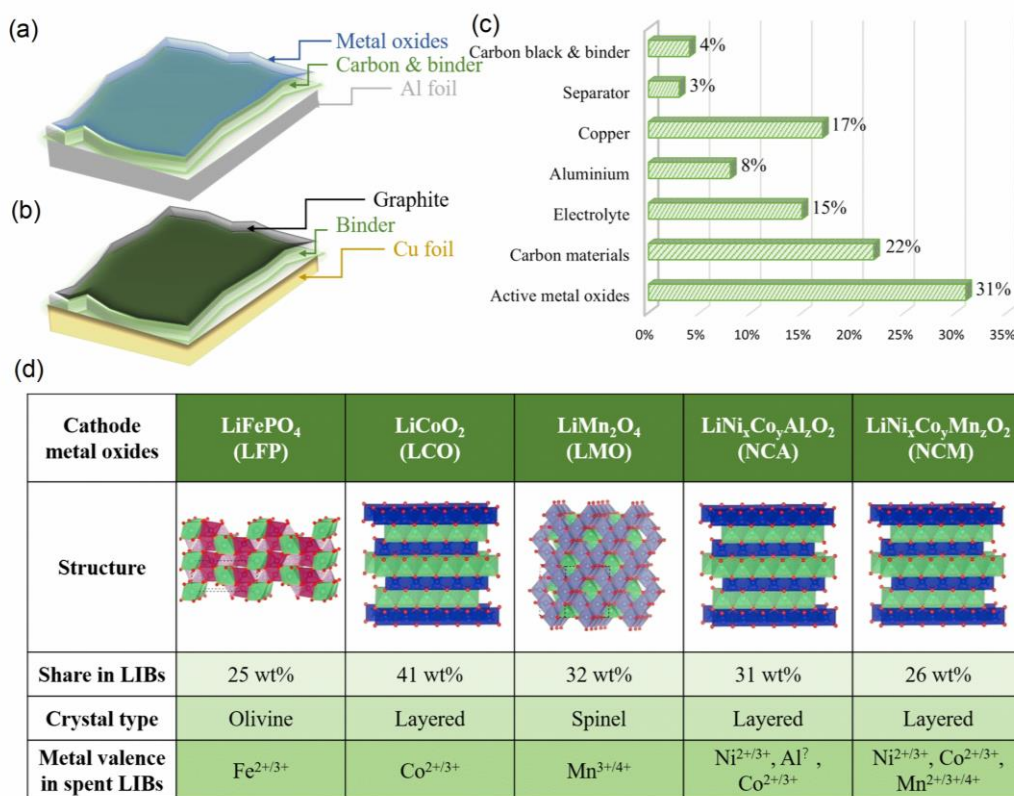


Figure 2. Composition of (a) cathode and (b) anode materials, (c) percentage of each components, and (d) comprehensive comparisons of cathode.

Usually, the generation of spent LIBs is caused by the deterioration of battery performance. Structural failure of electrode materials during cycling, severe shedding, dissolution, and dendrite accumulation phenomena are common causes of cell performance decay [40]. Furthermore, electrolyte leakage, decomposition, and cell short-circuiting can also diminish cell performance [41]. The components of LIBs, material structure, and metal valence may suffer from these factors. Typically, the cation mixing phenomenon may directly change the material structure and the metal valence state [42]. During the long-term charging and discharging process, some Li may be irreversibly de-embedded into graphite, while Ni, Co, Mn, and Fe in the cathode material may occupy Li positions. The structural and valence changes of metal oxides may lead to changes in adsorption characteristics and redox properties of active sites on the catalyst surface [43]. Therefore, suitable methods for the preparation of LIBs-based catalysts can maximize the utilization of inherent structures of electrodes and further improve catalyst performance.

2.2. Catalysts Preparation

To gain good catalytic performance and maximize economic efficiency, the preparation of catalysts usually focuses on the efficient use of valuable transition metals in the cathode material. For anode materials, graphite and copper foil are often recycled for further application. The comparison of different LIBs recovery methods is shown in Figure 3.

The preparation of LIBs-based catalysts is mainly a two-step process: the obtaining of cathode or anode materials (pretreatment) and the synthesis of high-performance catalysts. During the pre-treatment step, short-circuit explosions in LIBs and the negative effects of binder should be especially considered. Discharging is usually used to eliminate the remaining charge in LIBs, by immersing them in a salt solution (e.g., NaCl, MnSO₄, KCl, MgSO₄, FeSO₄, and NaNO₃) [44]. The main purpose of calcination is to remove binder from the material surface, given that the presence of binder is not conducive to the acquisition of cathode powder from aluminum foil. Furthermore, the catalytic performance of cathode

powder may be deteriorated due to the coverage of active sites on the catalyst surface by binder. Wang et al. investigated the effect of binder on the removal of sulfamethoxazole (SMX) by LFP-activated PMS. The results showed that the degradation rate of SMX was faster in the LFP/PMS system with a complete binder removal (100% during 30 min) than that without binder removal (79% during 150 min) [45]. In addition, binder removal methods include alkaline solution dissolution [45–47] and organic solution extraction methods [48,49]. Calcination is a more common method for binder removal, but overly high temperatures and different gas atmospheres (air roasting and anaerobic pyrolysis) may affect the material's structure and even destroy it. The choice of suitable operating conditions for different materials is particularly important. Generally, the temperature is controlled between 300 and 900 °C during the heat treatment [33].

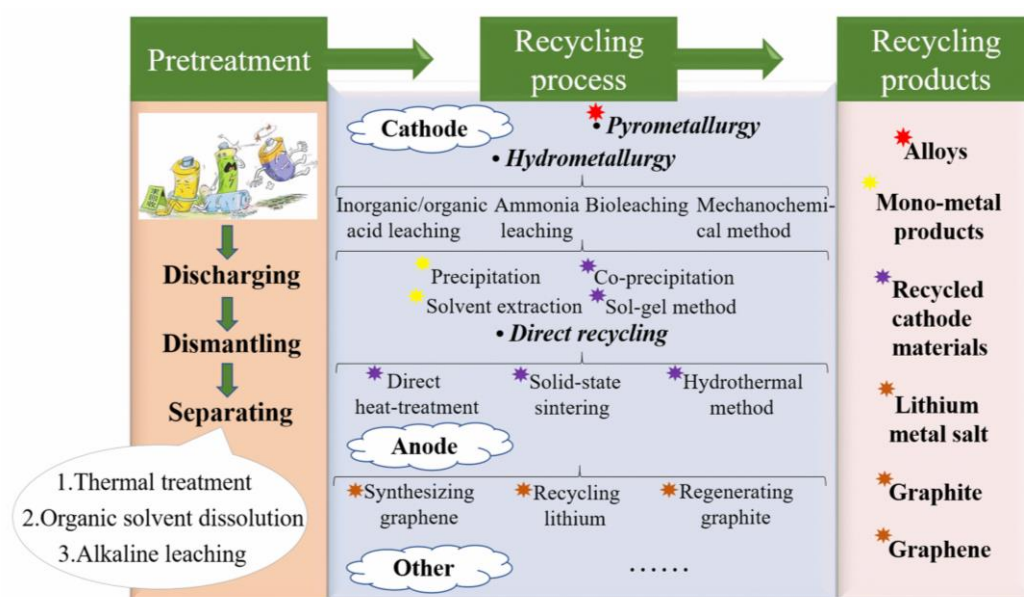
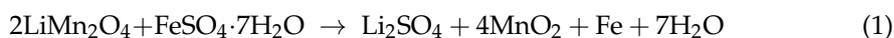


Figure 3. Comparison of different LIBs recovery methods.

The cathode material surface contains rich metal elements and surface oxygen, and it has the inherent advantage to be directly utilized as catalysts in catalytic reactions, such as transition metal catalysis [50,51], photocatalysis [52], and thermal catalysis [53]. Significantly, the lithium-ion loss during charging and discharging tends to cause structural changes in the electrode material, such as defects, distortions, or vacancies (cation vacancies and O_v) [18]. Defects and vacancies facilitate the improvement of active site quantities, electron transfer capacity, and oxygen adsorption capacity, thus providing better catalytic performance compared to pristine electrode materials [19,24]. In addition to the characteristics of their own structures, rich carbon resources (binder and conductive carbon in cathode materials and carbon materials in anode materials) are very favorable to enhance the catalyst adsorption capacity, and they should be considered in catalyst synthesis processes. Moreover, LIBs-based catalysts can be synthesized by other ways, such as doping, deposition, mechanical enhancement, etching, or heterogeneous synthesis. For example, the high-performance photocatalyst $MnO_2/Fe(0)$ was synthesized via the reaction of LMO and ferric sulphate heptahydrate (Equation (1)) [54]. The conversion of LMO to MnO_2 improved the electron transfer between substrates during $\bullet OH$ generation. The introduction of $Fe(0)$ further enhanced the degradation of sulphadiazine (SDZ) [55]. According to different requirements of catalyst performance, LIBs-based catalysts can be transformed into other transition metal oxides (CoO_x and MnO_x) [56]. In addition, these

transition metal oxides can be used as substrates and their catalytic performances can be further promoted by introducing specific metal elements (Co^{2+} , Cu^{2+} , and Ni^{2+}) [57].



Mechanical strengthening, acid treatment, and etching can facilitate the formation of O_v and cation vacancies by releasing metal ions from the material, which is beneficial to further promote the catalytic properties. Spent ternary battery-based catalysts (NCM 622) produced more O_v and cation vacancies by alkali etching, which achieved complete removal of propane at only 200 °C due to the enhanced lattice oxygen migration on the material surface and reduction capacity [58]. During mechanochemical activation, the cathode material suffers from mechanical friction and impact forces, thus becoming loose and small. Meanwhile, more O_v and cation vacancies are potentially created on material surfaces. Such a structure is conducive to the exposure of more active sites, which can facilitate catalytic reactions [59]. These methods suggest that catalytic decontamination can be effectively enhanced by changing the material structure. For metal heterojunction materials, it is characterized by good stability, high surface area, and high adsorption capacity. Particularly in the field of photocatalysis, good adsorption and photocatalytic capabilities greatly enhance the practical application ability [60,61]. Kumar et al. employed in situ deposition to synthesize LFP-based nanojunction photocatalysts, which are characterized by easy recovery (with magnetic properties), high visible-light absorption, and high adsorption [62]. In addition, the formation of conjugate structures is favorable for photocatalytic reactions, which can effectively reduce the electron transition energy and the reaction energy barrier by reducing the energy band gap and changing the material interlayer spacing [63].

3. Application in Catalytic Decontamination

3.1. Persulfate/Sulfite-Based AOPs

In recent years, persulfate-based AOPs have been widely used in water treatment due to the high removal efficiency, wide pH range, and high mineralization rate [64]. Typically, $\text{SO}_4^{\bullet-}$ can be generated by activation of peroxymonosulfate (PMS) or peroxydisulfate (PS) through transition metals over catalysts. $\text{SO}_4^{\bullet-}$ has a higher oxidation potential (2.5–3.1 V), longer half-life (30–40 us), and higher selectivity compared to other active species ($\bullet\text{OH}$, $\text{O}_2^{\bullet-}$, and $^1\text{O}_2$) [65]. Although both PMS and PDS are strong oxidizing agents and can produce $\text{SO}_4^{\bullet-}$ through activation by transition metal ions, cheaper PMS is more suitable for practical applications in the catalytic decontamination process.

LIBs-based catalysts activate PMS primarily through the electron transfer of transition metals on the catalyst surface. However, the great difference is reflected in the structure and catalytic performance of LIBs-based catalysts compared with traditional catalysts. Currently, LIBs-based catalysts for PMS activation are mainly divided into the direct application of electrode materials (after pretreatment) [45,59,66,67] and secondary synthesis (electrode materials are dissolved by inorganic acids to synthesize new catalysts by various methods, such as co-precipitation, hydrothermal, and sol-gel methods) [68–70]. Compared with secondary synthesis, direct application possesses simpler operation and higher economic efficiency, while it still has good catalytic properties for PMS activation due to its inherent structural advantages. On the one hand, the structure of electrode materials suffers from continuous lithiation/delithiation cycles during the charge/discharge process. Distortion and dislocation interspersed among crystal lattices, lattice expansion, and irreversible phase transition may be caused, which reduces the battery performance while possibly promoting PMS activation. For example, cracks (indicated by yellow circles in the figure) and folds on the material surface may lead to a decrease in transition metal valence and increase in adsorption capacity for contaminants (Figure 4a) [67,71]. The valence reduction of partial transition metals may be beneficial to decrease the consumption of PMS (self-decomposition or other competing reactions) by increasing the efficiency of redox reactions, while contaminants are more easily mineralized by being rapidly adsorbed on the catalyst surface. Similar findings were presented by Wang et al. and Dang et al. in their studies

of the LMO/PMS and NCM/PMS systems, respectively [50,72]. The generation of more O_V and metal vacancies can facilitate the adsorption of O_2 , electron transfer, and exposing more active sites during the activation of PMS, which contributes to the efficient utilization of PMS [50,72].

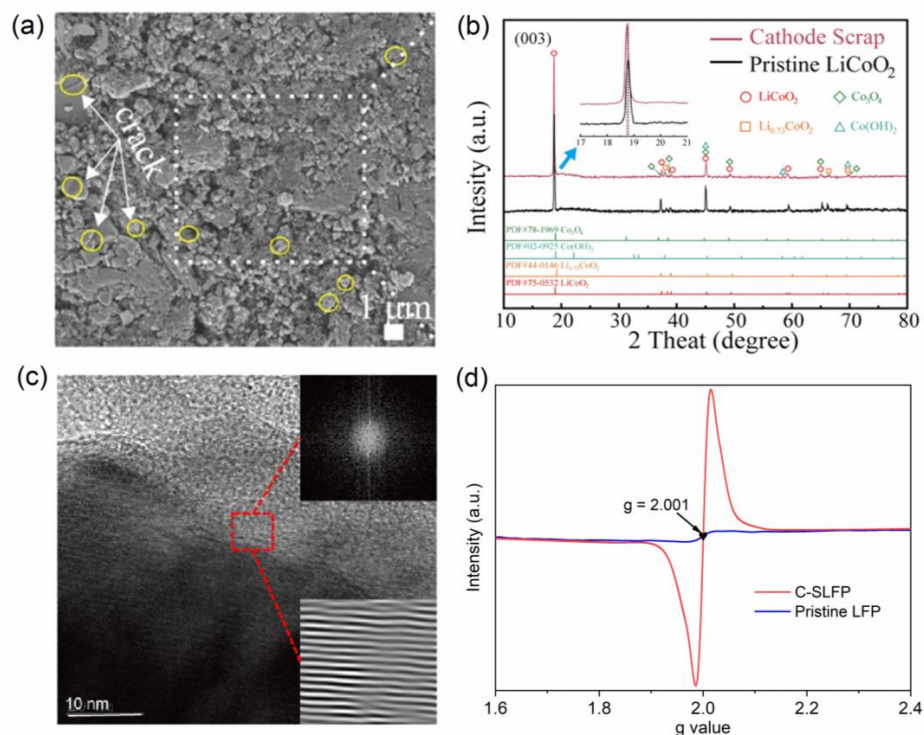


Figure 4. (a) SEM image of the recycled cathode scrap surface, (b) XRD patterns of pristine $LiCoO_2$ and cathode scrap, (c) the TEMs characterization of SLFP, and (d) EPR profiles of SLFP and pristine LFP catalysts. Reprinted with permission from Refs. [45,66,72].

On the other hand, the binder and conductive carbon during calcination (one of the pretreatment steps) may be effective to increase the specific surface area of LIBs-based catalysts by the self-decomposition of binder and the generation of gases [73,74]. More active sites could be exposed on the catalyst surface, which has a positive effect on systems with PMS. This was also found during a study of the NCM-650/PMS system by Zhao et al. [74]. The specific surface area of NCM-650 catalyst was significantly enhanced after calcination, which greatly improved the utilization of PMS in the catalytic decontamination process. This positive effect may be due to the increase in the number of exposed active sites, enhanced adsorption capacity, and oxidation capacity. In addition, the binder and conductive carbon on the LIBs-based catalysts surface during calcination may also cause a partial reduction in metal valence state through carbon-thermal reduction reactions. This effect may accelerate electron transfer between transition metals, thus accelerating the catalytic decontamination process [73].

Notably, vacancies and defects are not always present on the SLBEM surface, or the degree of scrap is not sufficient to promote catalytic reactions. Although those catalysts without inherent structural advantages after calcination treatment above $450\text{ }^\circ\text{C}$ may possess a modest catalytic capacity in catalytic decontamination [67,74,75], their catalytic efficiency for persistent organic pollutants is still inferior to that of SLBEMs with inherent structural advantages. The loss of lithium in the material may signify the presence of structural vacancies and defects. Typically, the shifts in characteristic peaks in X-ray diffraction (XRD) (Figure 4b) [24,66], the loss of lithium by inductively coupled plasma-atomic emission spectrometry (ICP-AES) testing, and the dislocation maps with the presence of distorted interlacing in transmission electron microscopy image (TEM) (Figure 4c) can

be used as primary diagnosis methods, while vacancies can be directly demonstrated by electron paramagnetic resonance (EPR) spectra (Figure 4d) [45,72]. Currently, there are two ways to enhance the catalytic performance of such “normal” LIBs-based catalysts, namely electrochemical enhancement and mechanochemical enhancement [50,59]. The changes in morphological structure (e.g., pore size, specific surface area, and particle size), metal vacancies, and O_v usually occur to improve catalytic performance during the strengthening process. Dang et al. successfully prepared LIBs-based catalysts using mechanochemical enhancement, and more active sites and vacancies were generated on LIBs-based catalysts surfaces during the mechanochemical enhancement [59]. It is noteworthy that the stability and decontamination efficiency of the enhanced catalyst are double those of pristine LCO, which is more suitable for practical applications.

Compared to persulfate, sulfite (S(IV)) is a common industrial contaminant, which is cheaper and more readily available. It has been documented that S(IV) can be activated using transition metals [76–82]. The process of the LIBs-based catalyst activating S(IV) for pollutant removal has good economic benefits and environmental protection significance. Typically, $SO_3^{\bullet-}$ is initially formed in the reaction process of S(IV) and transition metals, while $SO_3^{\bullet-}$ produces other active species through chain reactions [78,83–85]. Interestingly, PMS may be first generated in LIBs-based catalyst/S(IV) systems [24,86], which, in turn, is activated by transition metals on the catalyst surface to produce active species for pollutant removal. In the SLFP/S(IV) system, $SLFP \cdot O_2 \cdot SO_3H^-$ is predominantly generated through complexation of SLFP and S(IV), and, in turn, PMS is released into the system to participate in redox reactions (Equations (2) and (3)) [24,87,88]. Unlike the SLFP/S(IV) system, PMS is also generated initially in the LCO/S(IV) system, but the pathway of PMS generation is through two-step hydrogen shifts (Figure 5) [86].

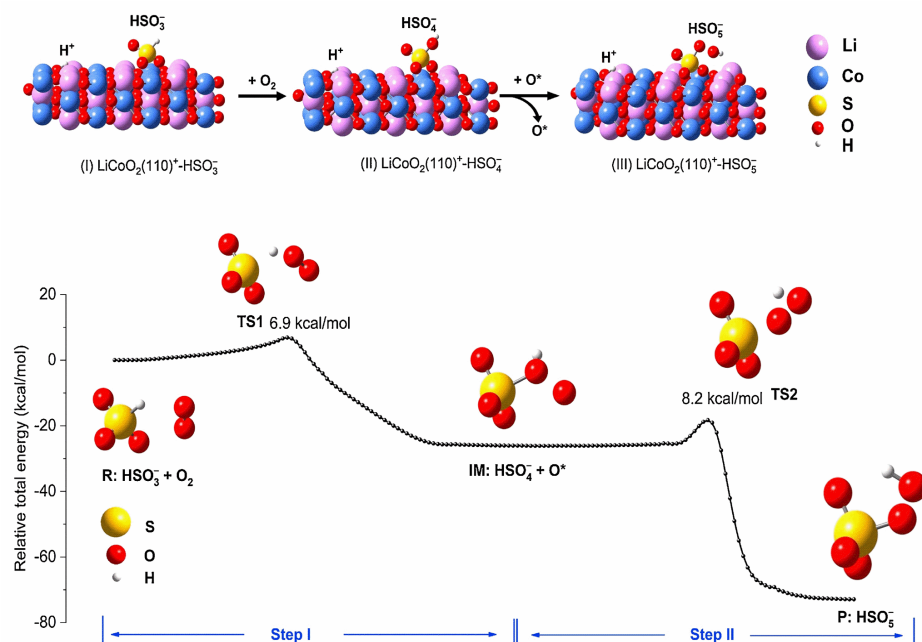
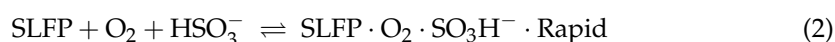


Figure 5. Adsorption structures of HSO_3^- , HSO_4^- , and HSO_5^- species on $LiCoO_2$ (110) surface as optimized by first-principles DFT calculations and potential energy profiles for two-step hydrogen shifts to form HSO_5^- during the reaction of HSO_3^- with O_2 by intrinsic reaction coordinate calculations. Structures of reactant (R), intermediate (IM), product (P), and transition states (TS) are shown near the curve. Reprinted with permission from Ref. [86].

3.2. Fenton-Like AOPs

The Fenton-like process has some advantages over the homogeneous Fenton reaction, such as wide pH range, good stability, and easy recovery of catalysts [89]. The heterogeneous Fenton reaction destructs organic pollutants mainly through the H₂O₂ activation by transition metals on the catalyst surface, which generates •OH with high oxidation capacity [90]. Currently, it has been studied that LIBs-based catalysts can provide a new strategy for the development of Fenton-like catalysts. However, the current research mainly focuses on the synthesis of new catalysts only by extracting transition metals from SLBEMs. The structural advantages of SLBEMs are not fully discovered. Usually, LIBs-based catalysts have good catalytic activity for H₂O₂ activation through the redox reaction of rich transition metals to produce highly oxidative •OH for water purification [44]. Abreu et al. fabricated LCO catalysts from cell phone batteries and established a LCO/H₂O₂ system for MB removal via electron transfer of Co(II)/Co(III) to activate H₂O₂ [44]. The degradation rate of MB was close to 100% within 150 min.

The electron transfer of transition metals (e.g., Fe(II)/Fe(III), Co(II)/Co(III), and Mn(II)/Mn(III)) is usually the main way to activate H₂O₂ in Fenton-like reactions. Notably, transition metals have low cycling efficiency in both homogeneous and heterogeneous systems. For example, the reaction rate between Fe(II) and H₂O₂ to Fe(III) ($k = 40\text{--}80 \text{ M}^{-1} \text{ s}^{-1}$) is much higher compared to the reaction of Fe(III) and H₂O₂ to Fe(II) ($k = 0.001\text{--}0.01 \text{ M}^{-1} \text{ s}^{-1}$) [91]. Some electron-rich materials have been used as reductants to accelerate the redox cycle of transition metals, thereby enhancing the catalytic performance of LIBs-based catalysts in catalytic decontamination processes. For example, carboxylates, carbon materials, metal sulfides, NH₂OH, and other reductive materials can significantly improve the Fenton reaction efficiency [92–96]. Zou et al. synthesized sea-urchin-like catalyst (SULM) as an activator of H₂O₂ (Figure 6a) [91]. The addition of NH₂OH effectively promoted the redox cycle of Fe(III)/Fe(II) on the SULM surface and Fe²⁺/Fe³⁺ in solution via the function of NH₃OH⁺, thus promoting the reactive oxygen species (ROS) generation (Figure 6b). The synergistic effect of surface and homogeneous reactions in the SULM + NH₂OH + H₂O₂ system was established for the removal of organic pollutants (Figure 6c). The degradation rate of RhB within 30 min was higher in the SULM + NH₂OH + H₂O₂ (100%) system compared to that of SULM + H₂O₂ (10%). Surprisingly, except for •OH, ¹O₂ was also supposed to be the main active oxidant during RhB removal. A few O₂^{•−} were detected by radical scavengers containing p-benzoquinone (BQ). The literature mentions that ¹O₂ and O₂^{•−} may be generated due to the coupling of •OH (Equation (4)) and the reaction between O₂ and Fe²⁺, respectively [96]. The same situation was not observed in other applications of LIBs-based catalysts, but a possibility was identified in favor of a more comprehensive consideration of degradation mechanisms in future studies.



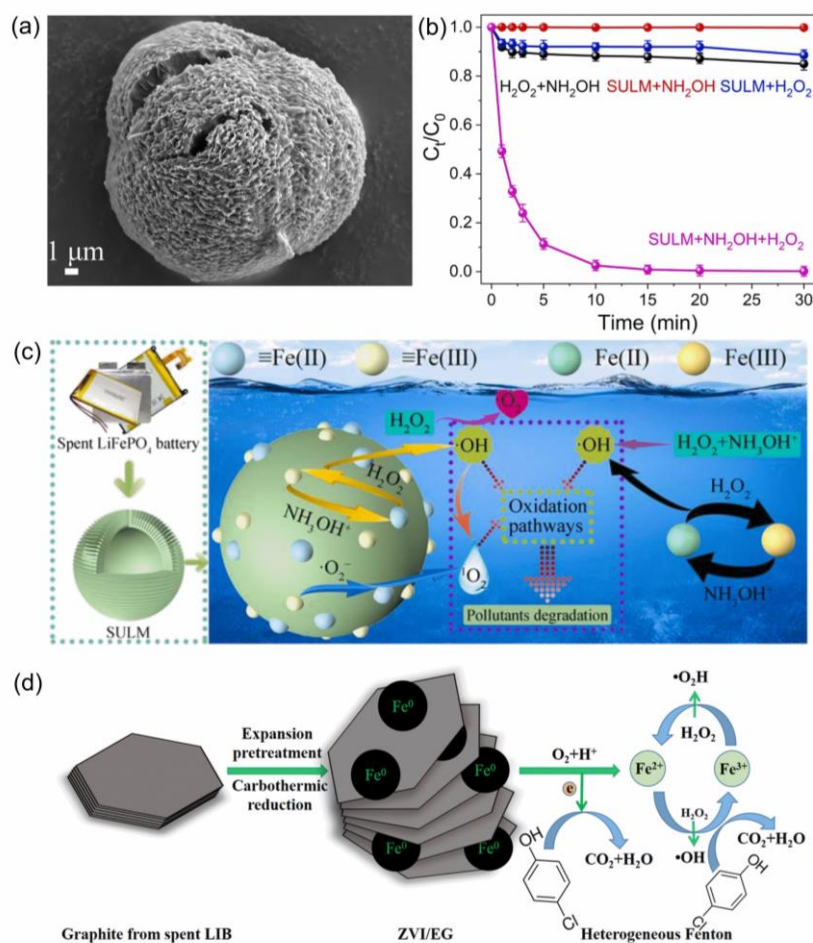


Figure 6. (a) The SEM image of SULM, (b) degradation efficiency of RhB in SULM + NH₂OH + H₂O₂ system, (c) schematic illustration of the production process and oxidation pathways of ROS, and (d) possible reaction mechanism of ZVI/EG system. Reprinted with permission from Refs. [91,97].

In addition, UV or visible light as energy is provided in the heterogeneous photo-Fenton to promote the formation of H₂O₂ and conversion of metal valence to enhance organic removal [98]. Moura et al. produced nanostructured catalysts (CoFe₂O₄-LIBs) for the activation of H₂O₂ by co-precipitation [21]. The MB removal rate was 87.7% in the CoFe₂O₄-LIBs system. Notably, additional H₂O₂ was generated during the catalytic process (Equations (5)–(8)). The combinational effects of photocatalysis and heterogeneous catalysis can effectively improve the activation efficiency of H₂O₂, accelerating the generation of free radicals and achieving rapid removal of pollutants. The carbon material of the anode in spent LIBs possesses a special advantage unlike the cathode material, which provides good carbon structures and conductivity. In particular, as a substrate, it has great potential for high-performance catalysts in diverse catalytic applications. Guan et al. successfully prepared zero-valent iron-loaded expanded graphite (ZVI/EG) using the carbothermal reduction method [97]. The synergistic effect of Fe(0) and the generated H₂O₂ in the ZVI/EG system effectively improved the decontamination efficiency (Figure 6d) [99–101]. The degradation rate of 4-CP reached 97% within 60 min. In addition, the EDS-mapping results of Fe before and after the reaction maintained a stable mass ratio. The degradation rate of 4-CP remained above 75% after 7 cycles. It can be seen that the good adsorption ability of the carbon material is beneficial to improve the catalyst stability in the catalytic decontamination process.





3.3. Thermocatalysis

Currently, the synthetic materials for LIBs-based thermocatalysts are mainly derived from spent LMO, NCM, and LCO. Although electrode materials are not used directly as thermocatalysts, they are still potentially useful for contaminant removal in terms of structural characteristics and material components. It is well known that O_v , the redox of transition metals (Mn^{3+}/Mn^{4+} , Cu^{2+}/Cu^{+} , Ni^{2+}/Ni^{3+} , and Co^{2+}/Co^{3+}), and metal vacancies (Li, Al, and Co) on the catalyst surface are favorable factors for the sustainable and effective removal of contaminants. LIBs-based catalysts possess innate structural advantages in catalytic applications that have been discussed and demonstrated in the above sections, such as efficient electron transfer capability, generation of defects and vacancies, and better adsorption capacity. This may have a positive impact on thermocatalytic decontamination.

The presence of lithium is usually detrimental to thermocatalytic reactions (Figure 7a). The reason is attributed to the probable cause of the reduction of oxygen species on the catalyst surface [102]. It is known that abundant oxygen species play an important role in thermal catalytic oxidation. It is especially important for systems where the removal of pollutants is dominated by surface-active oxygen oxidation. For example, LCO catalysts without excessive Li_2CO_3 have a higher efficiency for benzene removal compared to pristine LCO. The efficiency of benzene removal is greatly enhanced by exposing the bulk lattice oxygen on the catalyst surface due to removing excess Li_2CO_3 [53]. In the case of catalysts with inherent structural advantages, more loss of lithium ions may lead to more active sites on the catalyst surface, which facilitates thermocatalytic reactions. In addition, O_v and redox cycling of transition metals support the continuous replenishment of reactive oxygen species during thermocatalysis by capturing O_2 (Figure 7b) [23]. This may also be one of the positive effects of LIBs-based catalysts on thermocatalytic decontamination. The application of LIBs-based thermocatalysts with inherent defects is relatively rare compared to other application methods, which is perhaps the main reason why acid treatment and alkali etching are used as common treatment methods for generating vacancies and defects in catalyst structures [102–105].

Highly valent Mn (Mn^{4+}) has also been demonstrated to directly oxidize pollutants [106,107]. Although LIBs-based thermocatalysts contain abundant transition metals, most of the valence states of transition metals may be reduced after heat treatment due to carbon-thermal reduction reactions. In addition, the effects of other metals (e.g., Co^{2+} , Ni^{2+} , and Cu^{2+}) and acid treatment may also reduce the valence state of transition metals during the preparation of catalysts (Figure 7c) [23]. Fortunately, according to the principle of electroneutrality, low-valence Mn is closely related to the formation of O_v in thermocatalytic processes [108]. This greatly enhances the utilization value of LIBs-based catalysts. In addition, the good adsorption capacity of LIBs-based catalysts is equally important. LIBs-based catalysts containing carbon materials (conductive carbon and binder in cathode material and carbon material in cathode material) may have a large specific surface area. Unfortunately, the current research in LIBs-based thermocatalysts based on the innate structure of LIBs is less compared to other applications of LIBs-based catalysts. Although the structure and composition of SLBEMs may be relatively fixed compared to newly synthesized catalysts, the known structural advantages are still valuable for in-depth study. Furthermore, the comprehensive utilization of various components of LIBs in AOPs also deserves to be further explored.

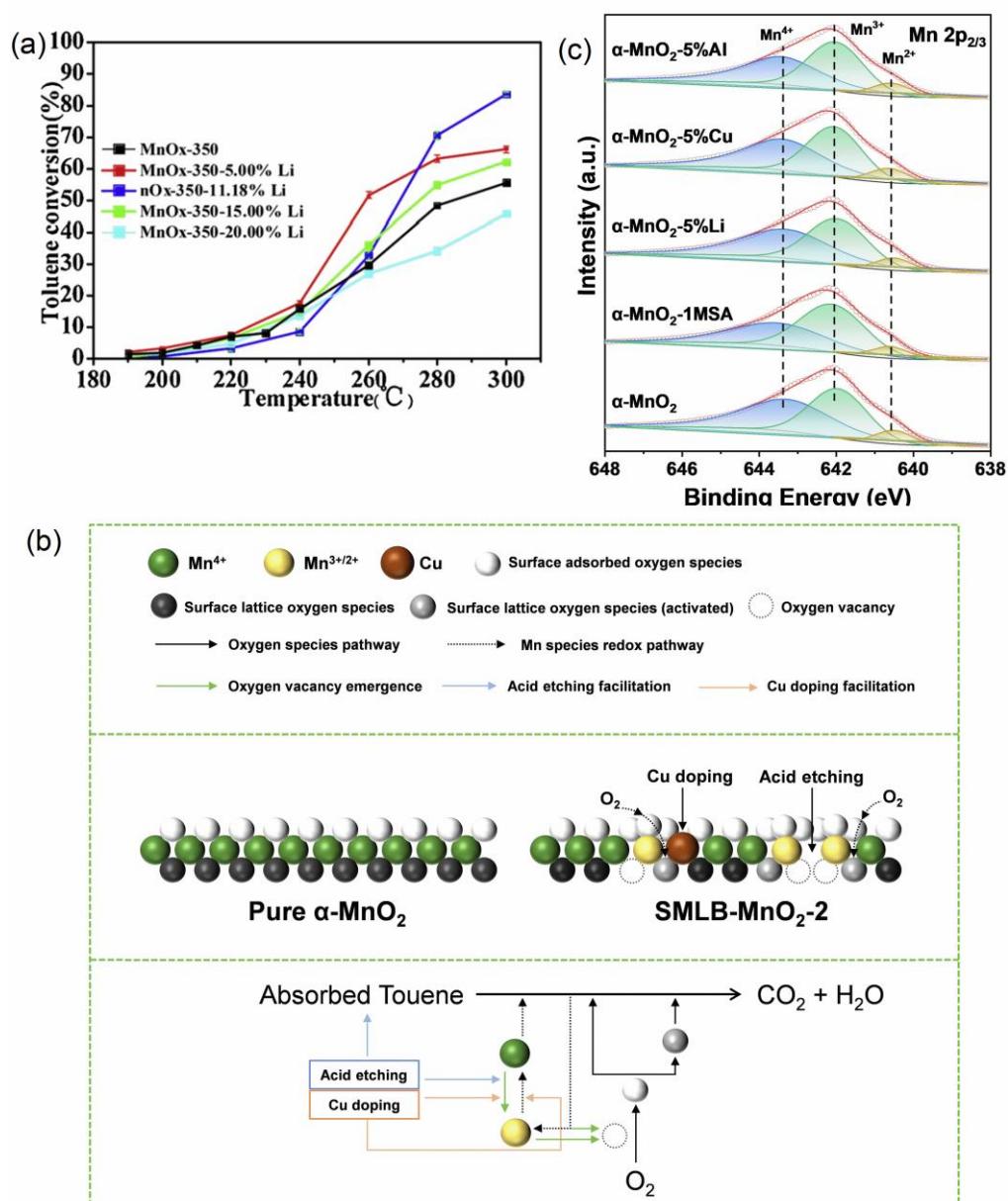


Figure 7. (a) The effect of different Li doping percentages on toluene oxidation, (b) proposed catalytic mechanism of toluene oxidation on SMLB-MnO₂-2, and (c) XPS spectra of Mn 2p_{3/2}. Reprinted with permission from refs. [23,102].

3.4. Photocatalysis

The application of LIBs-based catalysts in photocatalysis is slightly different compared to other applications. LIBs-based catalysts exhibit some unique structural advantages for catalytic reactions, but it cannot be directly applied in photocatalysis, due to its structural limitations. More critically, LIBs-based catalysts cannot be induced to produce a large number of hole–electron pairs under visible or UV light. For example, Guo et al. studied spent LFP for methyl orange (MO) removal by UV light [109]. The results are shown in Figure 8a, and MO was almost not degraded. The energy band gap of LFP (3.65 eV) has been reported to be much higher than that of g-C₃N₄ (2.7 eV) (a commonly used photocatalyst) [62]. LIBs-based catalysts cannot be directly applied in photocatalysis, probably due to their large energy band gap that inhibits hole–electron pair generation and electron migration.

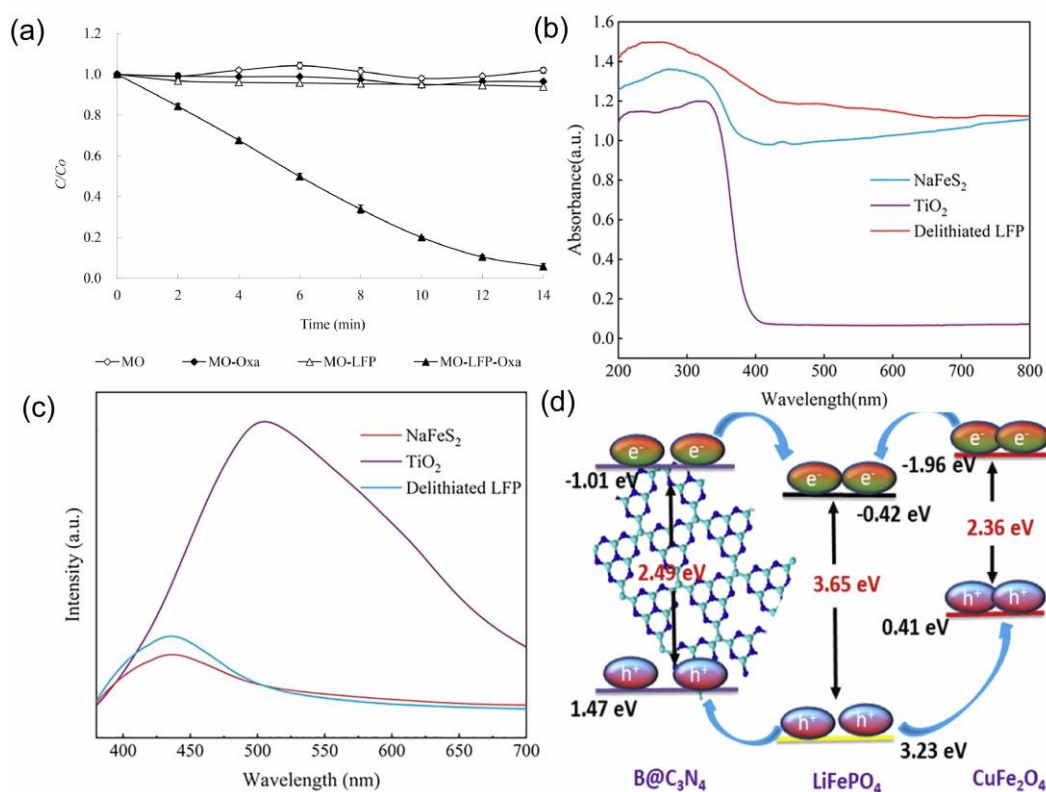


Figure 8. (a) Photodegradation of MO under varying conditions, (b) UV–vis diffuse reflectance spectra, (c) photoluminescence (PL) spectra, and (d) schematic diagram for charge separation and transfer in BLC–3 junction. Reprinted with permission from ref [25,62,109].

As is known, $g\text{-C}_3\text{N}_4$ is one of the most popular visible-light photocatalysts. Unfortunately, the practical applications of $g\text{-C}_3\text{N}_4$ face a challenge because of its low specific surface area, poor solar light utilization efficiency, and high recombination rate of photo-generated electrons and holes [110,111]. Moreover, the photocatalytic activity of TiO_2 is limited by two important drawbacks: the wide band gap (3.0–3.2 eV) resulting in the use of only UV light energy, and its low adsorption capacity for pollutants in solution [112,113]. Fortunately, LIBs-based catalysts possess good promotive effects for the photocatalytic performance of other catalysts (e.g., $g\text{-C}_3\text{N}_4$ and TiO_2), thus achieving efficient photocatalytic decontamination in practical applications. This facilitative effect mainly resulted from the structural characteristics of LIBs-based catalysts. As discussed in Section 3.1, LIBs-based catalysts may contain vacancies and defects due to the loss of lithium during charge and discharge, which facilitates photocatalytic decontamination. Surprisingly, de-lithiated LFP exhibited superior photocatalytic properties (wider photoabsorption boundary (200–800 nm), lower recombination rate, and lower photoluminescence intensity) compared to TiO_2 in photocatalytic applications (Figure 8c) [25,114,115]. Kumar et al. synthesized heterojunction photocatalysts [62] from LFP. The results revealed that the combination of LFP and other materials serve as a critical function in the enhancement of photocatalytic performance. Among them, the presence of structural defects in LFP is mainly responsible for greatly reducing the recombination rate. In addition, the band edges of LFP have a favorable position in the heterojunction catalyst (Figure 8d), which, in turn, promotes charge separation.

The carbon material in both anode and cathode electrodes may modify the structural morphology of photocatalysts (e.g., specific surface area and particle size), which would greatly enhance the removal ability for pollutants in photocatalytic decontamination [116]. Photocatalysis is an interfacial reaction; only when contaminants are diffused onto the surface of photocatalysts can they be degraded at a faster rate [117]. Therefore, good adsorp-

tion capacity is very critical for pollutant removal in photocatalytic processes. Moreover, the effective combination of abundant transition metals in anode materials with other photocatalysts may effectively reduce the energy band gap of photocatalysts. This beneficial effect may be attributed to the fact that embedding transition metals changes the structure of photocatalysts and, thus, promotes photocatalytic reactions. Niu et al. prepared a highly active photocatalyst through the effective combination of LCO and g-C₃N₄ [63]. The study found that the energy band gap of LIBs-based photocatalysts was significantly reduced from 0.92 eV to 0.27 eV due to the embedding of Co.

4. Key Factors Influencing Catalytic Activity

4.1. Initial Solution pH

The initial pH of the solution in LIBs-based catalytic reactions is more important for the catalytic performance of LIBs-based catalysts compared to other newly synthesized catalysts. This is mainly attributed to the relatively fixed structure and composition of LIBs-based catalysts. The activation of the oxidizing agent is mainly dependent on the redox reaction of the transition metal on the LIBs-based catalysts surfaces. Although vacancies and defects on the material surface can promote catalytic reactions, an unsuitable pH may inhibit the catalytic activity of the LIBs-based catalysts through the leaching of metal ions or passivation on the catalyst surface. Moreover, the catalyst surface charge, distribution of oxidizing agent, and target contaminant speciation are all likely to be influenced by pH [118]. Taking the LFP/S(IV) system for catalytic removal of BPS as an example [24], the highest degradation rate of BPS was observed at pH 3.0–5.0. At pH 6.0 and 7.0, the degradation rate of BPS became slow. BPS degradation was almost completely inhibited at pH 9.0 and 11.0. Considering the isotropic point of LFP (pH_{ZPC} = 5.8), the S(IV) speciation (HSO₃[−]/SO₃^{2−}), and the BPS dissociation constants (pK_{a,1} = 7.42, pK_{a,2} = 8.03) [119], at pH > 5.8, the LFP surface is negatively charged, with BPS in the anionic state (BPS[−]/BPS^{2−}) and SO₃^{2−} being the predominant forms. Therefore, the degradation efficiency of BPS is negatively affected mainly due to the electrostatic repulsion between the species. The precipitation of Fe(OH)₃ on the material surface under alkaline conditions may also lead to the LFP poisoning [78]. In addition, pH determines the type and level of active oxidizing species in the catalytic decontamination process. Under alkaline conditions, large amounts of OH[−] may react with the SO₄^{•−} in water, contributing to the production of •OH (Equation (9)) [120]. In addition, the pH effect is also present in the photocatalytic process. At lower pH conditions, h⁺ is preferentially formed compared to •OH. Conversely, when the pH is neutral or basic, •OH plays a key role in catalytic decontamination [121,122]. Evidently, selection of the appropriate pH has a direct impact on the catalyst activity for the contaminant removal.



4.2. Reaction Temperature

For thermal catalysis, the relationship between catalytic performance and reaction temperature of different LIBs-based thermocatalysts is compared (Table 1). Remarkably, the contaminants can be rapidly degraded only when the reaction temperatures reach a certain critical temperature. This may be attributed to different surface activation energies (E_a) for contaminant oxidation over the catalyst [123]. The thermocatalytic decontamination process is accelerated when the reaction temperature meets E_a required by the LIBs-based thermocatalysts. Moreover, the relationship between reaction temperature and pollutant removal is usually positively correlated in AOPs. For example, Liu et al. investigated the catalytic oxidation of benzene VOCs by LCO [60]. Only 40% of pollutants were removed at reaction temperatures ranging from 0 °C to 200 °C, while pollutants were completely removed when the temperature was increased to 500 °C. Guo et al. prepared manganese-based catalysts from LMO for enhancing VOC removal [106]. The decay of 1-methoxy-2-propyl acetate (MPA) also reflected a positive correlation between reaction temperature and pollutant removal. A similar trend was observed in Fenton-like catalytic reactions

where the decay of organic pollutants and the decomposition of H_2O_2 were higher at 60 °C as compared to 20 °C [124].

Table 1. The relationship between catalytic performance of different LIBs-based thermocatalysts and temperature.

Catalysts	I_{ct}^a	T_{50}^b	T_{90}^b	Pollutants	Ref
SLMB-MnO ₂ -2	1000	208	224	Toluene	[23]
H ₂ O-LCO	407–467	250	430	Airborne benzene	[60]
MnO _x (SY)-0.1	1000	150	180	2-ethoxy-ethanol	[102]
GdMnO ₃ (SY)-0.05	1000	190	220	2-ethoxy-ethano	[102]
SmMnO ₃ -STLIB	1000	208	244	Propylene glycol methyl	[103]
SmCoO ₃ -STLIB	1000	216	307	Propylene glycol methyl	[103]
MnO _x (MS)/CeO ₂ -C	1000	196	253	2-ethoxyethyl acetate	[104]
CoO _x (GS)/CeO ₂ -P	1000	194	253	2-ethoxyethyl acetate	[104]
MnO _x (SY)/CeO ₂ -C	1000	179	222	2-ethoxyethyl acetate	[104]
MnO _x -M-350	1000	243	290	Toluene	[105]
MnO _x -M-5% Fe	1000	174	212	1-methoxy-2propyl-acetate	[106]
MnO _x -M-10% Ce	1000	192	224	1-methoxy-2propyl-acetate	[106]
MnO _x -M-15% Bi	1000	184	214	1-methoxy-2propyl-acetate	[106]
MnO _x (SY)(HT)	1000	181	218	1-methoxy-2-propanol	[107]
CoO _x (GS)(CP)	1000	180	213	1-methoxy-2-propanol	[107]
Co _{3-x} M _x O ₄ -500	1000	247	274	Toluene	[125]
H-LiCo	370–430	215	250	Airborne benzene	[126]
AgHPWLiCo	450–480	225	275	Airborne benzene	[127]

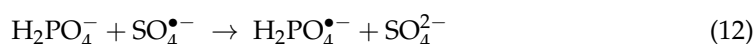
^a Initial concentration (ppm) of organic pollutants; ^b the temperatures corresponding to 90% (T_{90} , °C) and 50% (T_{50} , °C) of organic pollutants.

4.3. Coexisting Anions

LIBs-based catalysts may also be influenced in practical applications by the large number of anions and humic acid (HA) in the actual wastewater, such as CO_3^{2-} , HCO_3^- , Cl^- , NO_3^- , H_2PO_4^- , and HA [128]. In general, the anions and HA in the practical water body are quenchers for active radicals. The decrease in reactive radicals leads to a decrease in the efficiency of organic pollutant removal. In addition, the inhibitory degree of pollutant removal by anions and HA is positively correlated with their concentration. Zhao et al. prepared NCM-650 catalyst for PMS activation [74] and found that pollutant removal declined continuously (100% to 80%) when the anion and HA concentrations in solution increased (0 mM to 20 mM). NO_3^- , Cl^- , HCO_3^- , and HA all had inhibitory effects on pollutant removal. This may be due to the part of reactive radicals ($\bullet\text{OH}$ and $\text{SO}_4^{\bullet-}$) in solution being quenched (Equations (10)–(13)) [129–131]. In addition, the alkaline environment generated by the HCO_3^- hydrolysis leads to electrostatic repulsion between NCM-650 and PMS, which inhibits the removal of contaminants [132]. A similar trend was observed in a study by Dang et al. for the effects of NO_3^- , Cl^- , HCO_3^- , and HA. The reactive radicals in solution were depleted and a large number of less oxidizing reactive species (Cl^\bullet , $\text{HCO}_3^{\bullet-}$, $\text{CO}_3^{\bullet-}$, and $\text{H}_2\text{PO}_4^{\bullet-}$) were generated [59]. Apart from quenching the active radicals, H_2PO_4^- may also chelate with the active sites on the catalyst surface, diminishing active sites available for PMS activation [133].

Especially, the addition of high concentrations of Cl^- is likely to promote contaminant degradation in some cases. For example, the addition of Cl^- (100 mM) promoted the complete degradation of BPA compared to the absence of Cl^- [69]. Cl^- in solution is directly oxidized by PMS to form reactive chlorine (e.g., Cl_2 and HOCl) (Equations (14) and (15)), which facilitates the contaminant degradation. In other words, BPA was degraded by both reactive radicals and reactive chlorine [134,135]. Notably, Cl^- facilitates or inhibits catalytic reactions depending on diverse factors. The efficient degradation of BPA is mainly due to the action of Cl_2 and HOCl and the presence of the electron-donating hydroxyl group on the benzene ring. The elevated Cl^- concentration gives the opportunity for Cl_2 and HOCl to be generated by the chain reaction of excess Cl^- . The excessive amounts of Cl_2

and HOCl can mineralize the electron-rich BPA and improve the efficiency of BPA removal through hydrogen extraction and single-electron oxidation. The concentration of Cl^- , rate constants between the radicals ($\bullet\text{OH}$, $\text{SO}_4^{\bullet-}$, and halogen radicals) and between radicals and target organic pollutants, experimental operating conditions, and unique structures of pollutants (containing electron-donating groups and electron-withdrawing groups) can have different effects on the removal of contaminants in the presence of Cl^- [136]. Therefore, choosing suitable degradation methods and specifying types of pollutant structures should be considered in catalytic decontamination processes when faced with the co-existence of pollutants and anions in actual wastewater.



4.4. Catalyst Dosage

The catalyst dosage is one of the key factors in the catalytic decontamination process. High catalyst concentration will provide more reactive sites and accelerate the catalytic reaction process. However, when too much catalyst is used, the transition metals on the catalyst surface quench the active radicals, leading to the reduction in pollutant removal efficiency [137]. In addition, the catalyst itself may undergo agglomeration, affecting the catalytic efficiency. For example, catalyst agglomeration in photocatalysis may reduce the light transmission capacity [8]. Therefore, both economic efficiency and pollutant removal efficiency should be considered while selecting the optimal catalyst dosage.

4.5. Possible Problems in Practical Decontamination

The rapid development of LIBs-based catalysts is expected to effectively relieve the pressure on e-waste recycling and environmental protection processes. Facing the complex water treatment environment in practical application processes, catalysts with high stability, good catalytic ability, low cost, and easy preparation are required. In terms of LIBs-based catalysts, some possible issues should be further investigated in the future.

First, some innate structural advantages of spent LIBs have been proven to facilitate the catalytic decontamination process. However, based on the application of LIBs-based catalysts, we found that not all structures of spent LIBs are favorable for improving catalytic performance. Therefore, the relationship between the degree of scrap and structural advantages of spent LIBs should be more clearly defined, or assessed by some indicators for spent LIBs. This helps to fully utilize the catalytic value of LIBs-based catalysts in actual catalytic decontamination. Secondly, the idea of preparing catalysts at the current stage may be influenced by the traditional recovery methods of LIBs. The new catalyst was synthesized only by extracting transition metals from SLBEMs before the structural advantages of materials were clearly recognized. The method of extracting transition metals is basically the same as conventional recovery ideas. High costs, complex operations, and hazards of secondary contamination may still be created while the value of SLBEMs is not maximized. This is contradictory to the goal of greener and higher-value recycling of spent LIBs. Thirdly, the stability of LIBs-based catalysts at different pH needs to be further improved. The transition metals on LIBs-based catalyst surfaces play a key role in the catalytic decontamination process, while pH may cause catalyst surface passivation, protonation, de-protonation, and changes in surface charge (positive or negative), which further affect the catalytic decontamination performance.

5. Conclusions and Outlooks

In recent years, the recycling of spent LIBs has gained widespread attention due to their large end-of-life quantities and possible hazards. In particular, cathode materials with large amounts of valuable metal and anode materials with abundant carbon sources may process an inherent advantage in catalytic decontamination. Several studies have focused on the utilization of SLBEMs as efficient catalysts for photocatalysis, transition metal catalysis, and thermocatalysis. Further efforts are needed for the utilization and metal recycling of SLBEMs.

First, the safety and greenness of recycling spent LIBs electrode material before utilization should be considered. Pretreatment is critical to obtain high-performance catalyst precursors and its negative effects may cause changes in catalyst structure and surface metal valence (metal oxidation or surface passivation), which may directly affect subsequent catalyst synthesis or efficient catalytic performance. Moreover, leaching, acid treatment, and alkali etching treatments should be reduced or replaced by other methods, which would effectively avoid environmental pollution. High-temperature calcination could be a promising method for metal separation. In addition, the recovery of lithium can be considered as an additional profit in the preparation of catalysts. On the one hand, its development facilitates the maximization of economic efficiency. On the other hand, more active sites and vacancies may be exposed on catalyst surface during lithium removal, thus improving catalytic performance. Therefore, the lithium extraction process could be considered to develop in terms of both enhanced catalytic performance and economic efficiency. LIBs-based catalysts can be reused but not permanently maintain high performance in catalytic decontamination, and consideration for its final fate is necessary in future development. Compared to catalyst regeneration technologies, recovery of valuable metals may be more important to maximize the economic benefits of recycling spent LIBs while reducing environmental pollution.

Secondly, the synthesis of LIBs-based catalysts is more often carried out by hydrometallurgy than by pyrometallurgy. Hydrometallurgy may result in positive effects (e.g., O_v , metal defects, and more active sites) on transition metal oxides in catalytic applications, especially in catalytic decontamination. Other transition-metal-based compounds with excellent properties (e.g., sulfide, nitride, and phosphide) are to be developed further. For example, the electrostatic interaction between negatively charged S^{2-}/S_2^{2-} and positively charged MB on the $NaFeS_2$ surface greatly contributes to the adsorption and removal efficiency of MB. In addition, LIBs-based catalysts or composite catalysts still face significant challenges in catalytic decontamination due to the complexity of the actual application environment (co-existing anions, other organic pollutants, and pH). Therefore, while the catalytic decontamination capability of LIBs-based catalysts is increasing, the practical application capability should also be emphasized and enhanced.

Finally, apart from the extra addition of other substances, the components of the waste LIBs themselves (e.g., graphite, copper foil, and aluminium foil) need to be utilized effectively and combined with each other in appropriate ways. For example, adopting aluminum foil as a reducing agent greatly enhances the catalytic performance of LCO for PMS through mechanochemical activation, producing O_v and metal vacancies that facilitate catalytic decontamination. The anode contains abundant graphite, which is the main material for the production of graphene. Graphene, which is characterized by good electrical properties, large specific surface area, and stability, can be used as a conductive additive or catalyst substrate. These strategies of LIBs-based catalyst preparation will provide considerable effectiveness toward efficient environmental protection and catalytic material synthesis. The combination of diversified utilization of clean energy (e.g., light, hydrogen, and wind) and reduced energy consumption (e.g., low-temperature thermal catalysis, carbon capture, and carbon utilization) in the catalytic decontamination process can be considered as a future development direction, which can better achieve the strategic goal of “treating waste to waste” in the process of e-waste resource recovery.

Author Contributions: Data curation, P.W.; writing—original draft preparation, P.W.; writing—review and editing, P.W., J.G., Y.G. and Z.W.; funding acquisition, Z.W. All authors have read and agreed to the published version of the manuscript.

Funding: This work was supported by the Natural Science Foundation of China (52070127; 52270129), the Science and Technology Innovation Action Plan of Shanghai under the Belt and Road Initiative (No. 19230742800), the Shanghai Natural Science Foundation (20ZR1421100), and the Science and Technology Development Fund of Pudong New Area (PKJ2021-C01).

Data Availability Statement: No available data.

Conflicts of Interest: The authors declare no conflict of interest.

References

1. Jung, J.C.; Sui, P.; Zhang, J.J. A review of recycling spent lithium-ion battery cathode materials using hydrometallurgical treatments. *J. Energy Storage* **2021**, *35*, 102217. [[CrossRef](#)]
2. Liu, J.J.; Shi, H.; Hu, X.; Geng, Y.N.; Yang, L.M.; Shao, P.H.; Luo, X.B. Critical strategies for recycling process of graphite from spent lithium-ion batteries: A review. *Sci. Total. Environ.* **2022**, *816*, 151621. [[CrossRef](#)] [[PubMed](#)]
3. Makuza, B.; Tian, Q.H.; Guo, X.Y.; Chattopadhyay, K.; Yu, D.Y. Pyrometallurgical options for recycling spent lithium-ion batteries: A comprehensive review. *J. Power Sources* **2021**, *491*, 229622. [[CrossRef](#)]
4. Zhao, Y.L.; Yuan, X.Z.; Jiang, L.B.; Wen, J.; Wang, H.; Guan, R.P.; Zhang, J.J.; Zeng, G.M. Regeneration and reutilization of cathode materials from spent lithium-ion batteries. *Chem. Eng. J.* **2021**, *383*, 123089. [[CrossRef](#)]
5. Zhang, H.X.; Song, Y.Y.; Nengzi, L.C.; Gou, J.F.; Li, B.; Cheng, X.W. Activation of persulfate by a novel magnetic $\text{CuFe}_2\text{O}_4/\text{Bi}_2\text{O}_3$ composite for lomefloxacin degradation. *Chem. Eng. J.* **2020**, *379*, 122362. [[CrossRef](#)]
6. Yang, Z.; Li, Y.; Zhang, X.; Cui, X.; He, S.; Liang, H.; Ding, A. Sludge activated carbon-based CoFe_2O_4 -SAC nanocomposites used as heterogeneous catalysts for degrading antibiotic norfloxacin through activating peroxydisulfate. *Chem. Eng. J.* **2020**, *384*, 123319. [[CrossRef](#)]
7. Liu, X.; Li, C.S.; Zhang, Y.; Yu, J.Y.; Yuan, M.; Ma, Y.Q. Simultaneous photodegradation of multi-herbicides by oxidized carbon nitride: Performance and practical application. *Appl. Catal. B* **2017**, *219*, 194–199. [[CrossRef](#)]
8. Guan, K.; Zhou, P.J.; Zhang, J.Y.; Zhu, L.L. Synthesis and characterization of $\text{ZnO}@\text{RSDBC}$ composites and their Photo-Oxidative degradation of Acid Orange 7 in water. *J. Mol. Struct.* **2020**, *1203*, 127425. [[CrossRef](#)]
9. Osegueda, O.; Dafinov, A.; Llorca, J.; Medina, F.; Sueiras, J. Heterogeneous catalytic oxidation of phenol by in situ generated hydrogen peroxide applying novel catalytic membrane reactors. *Chem. Eng. J.* **2015**, *262*, 344–355. [[CrossRef](#)]
10. Guan, K.; Zhou, P.J.; Zhang, J.Y.; Zhu, L.L. Catalytic degradation of acid orange 7 in water by persulfate activated with $\text{CuFe}_2\text{O}_4@\text{RSDBC}$. *Mater. Res. Express.* **2020**, *7*, 016529. [[CrossRef](#)]
11. Akerdi, A.G.; Bahrami, S.H. Application of heterogeneous nano-semiconductors for photocatalytic advanced oxidation of organic compounds: A review. *J. Environ. Chem. Eng.* **2019**, *7*, 103283. [[CrossRef](#)]
12. Hu, P.D.; Long, M.C. Cobalt-catalyzed sulfate radical-based advanced oxidation: A review on heterogeneous catalysts and application. *Appl. Catal. B* **2016**, *181*, 103–117. [[CrossRef](#)]
13. Liu, Z.Z.; Yang, S.J.; Yuan, Y.N.; Xu, J.; Zhu, Y.F.; Li, J.J.; Wu, F. A novel heterogeneous system for sulfate radical generation through sulfite activation on a CoFe_2O_4 nanocatalyst surface. *J. Hazard. Mater.* **2016**, *10*, 18183. [[CrossRef](#)] [[PubMed](#)]
14. Cheng, J.H.; Lu, T.; Huang, S.Q.; Li, G.B.; Wang, J.; Kong, F.; Cheng, Q.L.; Zhang, Y.H. Recovery of cobalt spent lithium-ion batteries as the dopant of TiO_2 photocatalysts for boosting ciprofloxacin degradation. *J. Clean. Prod.* **2021**, *316*, 128279. [[CrossRef](#)]
15. Min, X.; Guo, M.M.; Liu, L.Z.; Li, L.; Gu, J.N.; Liang, J.X.; Chen, C.; Li, K.; Jia, J.P.; Sun, T.H. Synthesis of MnO_2 derived from spent lithium-ion batteries via advanced oxidation and its application in VOCs oxidation. *J. Hazard. Mater.* **2021**, *406*, 124743. [[CrossRef](#)]
16. Jacoby, M. It's time to get serious about recycling lithium-ion batteries. *Chem. Eng. News.* **2019**, *97*, 28.
17. Golubkov, A.; Fuchs, W.D.; Wagner, J.; Wiltsche, H.; Stangl, C.; Fauler, G.; Voitic, G.; Thaler, A.; Hacker, V. Thermal-runaway experiments on consumer Li-ion batteries with metal-oxide and olivin-type cathodes. *RSC Adv.* **2014**, *4*, 3633. [[CrossRef](#)]
18. Xu, B.; Dong, P.; Duan, J.; Wang, D.; Huang, X.; Zhang, Y. Regenerating the used LiFePO_4 to high performance cathode via mechanochemical activation assisted V^{5+} doping. *Ceram. Int.* **2019**, *45*, 11792–11801. [[CrossRef](#)]
19. Ji, J.; Aleisa, R.; Duan, H.; Zhang, J.; Yin, Y.; Xing, M. Metallic active sites on MoO_2 (110) surface to catalyze advanced oxidation processes for efficient pollutant removal. *Iscience* **2020**, *23*, 100861. [[CrossRef](#)]
20. Yi, C.; Zhou, L.; Wu, X.; Sun, W.; Yi, L.; Yang, Y. Technology for recycling and regenerating graphite from spent lithium-ion batteries. *Chin. J. Chem. Eng.* **2021**, *39*, 37–50. [[CrossRef](#)]
21. Moradi, B.; Botte, G.G. Recycling of graphite anodes for the next generation of lithium ion batteries. *J. Appl. Electrochem.* **2016**, *46*, 123–148. [[CrossRef](#)]
22. Moura, M.N.; Barrada, R.V.; Almeida, J.R.; Moreira, T.F.M.; Schettino, M.A.; Freitas, J.C.C.; Ferreira, S.A.D.; Lelis, M.F.F.; Freitas, M.B.J.G. Synthesis, characterization and photocatalytic properties of nanostructured CoFe_2O_4 recycled from spent Li-ion batteries. *Chemosphere* **2017**, *182*, 339–347. [[CrossRef](#)] [[PubMed](#)]

23. Min, X.; Guo, M.M.; Li, K.; Gu, J.; Hu, X.F.; Jia, J.P.; Sun, T.H. Boosting the VOCs purification over high-performance α -MnO₂ separated from spent lithium-ion battery: Synergistic effect of metal doping and acid treatment. *Sep. Purif. Technol.* **2022**, *295*, 121316. [[CrossRef](#)]
24. Wang, P.; Lou, X.Y.; Sun, X.H.; Chen, Q.Q.; Liu, Y.J.; Guo, Y.G.; Zhang, X.J.; Guan, J.; Wang, R.X.; Zhang, R.; et al. Spent rather than pristine LiFePO₄ cathode materials can catalytically activate sulfite for organic pollutants decontamination. *Chem. Eng. J.* **2022**, *446*, 137123. [[CrossRef](#)]
25. Yue, X.H.; Zhang, F.S. Recycling spent LiFePO₄ battery for fabricating visible-light photocatalyst with adsorption-photocatalytic synergistic performance and simultaneous recovery of lithium and phosphorus. *Chem. Eng. J.* **2022**, *450*, 138388. [[CrossRef](#)]
26. Golmohammadzadeh, R.; Faraji, F.; Rashchi, F. Recovery of lithium and cobalt from spent lithium ion batteries (LIBs) using organic acids as leaching reagents: A review. *Resour. Conserv. Recy.* **2018**, *136*, 418–435. [[CrossRef](#)]
27. Xu, B.; Qian, D.; Wang, Z.Y.; Meng, Y.S. Recent progress in cathode materials research for advanced lithium ion batteries. *Mat. Sci. Eng. R.* **2012**, *73*, 51–65. [[CrossRef](#)]
28. Xiao, J.; Li, J.; Xu, Z. Challenges to future development of spent lithium ion batteries recovery from environmental and technological perspectives. *Environ. Sci. Technol.* **2020**, *54*, 9–25. [[CrossRef](#)] [[PubMed](#)]
29. Liu, P. Recycling waste batteries: Recovery of valuable resources or reutilization as functional materials. *ACS Sustain. Chem. Eng.* **2018**, *6*, 11176–11185. [[CrossRef](#)]
30. Zhang, X.; Li, L.; Fan, E.; Xue, O.; Bian, Y.; Wu, F.; Chen, R. Toward sustainable and systematic recycling of spent rechargeable batteries. *Chem. Soc. Rev.* **2018**, *47*, 7239–7302. [[CrossRef](#)] [[PubMed](#)]
31. Jin, Y.C.; Zhang, T.; Zhang, M.D. Advances in intelligent regeneration of cathode materials for sustainable lithium-ion batteries. *Adv. Energy Mater.* **2022**, *12*, 2201526. [[CrossRef](#)]
32. Shen, Y.F. Recycling cathode materials of spent lithium-ion batteries for advanced catalysts production. *J. Power Sources* **2022**, *528*, 231220. [[CrossRef](#)]
33. Niu, B.; Xiao, J.F.; Xu, Z.M. Advances and challenges in anode graphite recycling from spent lithium-ion batteries. *J. Hazard. Mater.* **2022**, *439*, 129678. [[CrossRef](#)] [[PubMed](#)]
34. Costa, C.M.; Barbosa, J.C.; Goncalves, R.; Castro, H.; Del Campo, F.J.; Lanceros-Méndez, S. Recycling and environmental issues of lithium-ion batteries: Advances, challenges and opportunities. *Energy Storage Mater.* **2021**, *37*, 433–465. [[CrossRef](#)]
35. Tian, G.D.; Yuan, G.; Aleksandrov, A.; Zhang, T.; Li, Z.W.; Fathollahi-Fard, A.M.; Ivanov, M. Recycling of spent lithium-ion batteries: A comprehensive review for identification of main challenges and future research trends. *Sustain. Energy Technol.* **2022**, *53*, 102447. [[CrossRef](#)]
36. Du, K.D.; Wu, X.L.; Liu, Y.C. Progresses in sustainable recycling technology of spent lithium-ion batteries. *Energy Environ. Mater.* **2022**, *5*, 1012–1036. [[CrossRef](#)]
37. Leal, V.M.; Ribeiro, J.S.; Coelho, E.L.D.; Freitas, M.B.J.G. Recycling of spent lithium-ion batteries as a sustainable solution to obtain raw materials for different applications. *J. Energy Chem.* **2022**, *in press*. [[CrossRef](#)]
38. Gaines, L.; Spangenberg, J.; Dai, Q. Lithium-ion battery recycling process comparison. *Meet. Abstr.* **2018**, *5*, 605. [[CrossRef](#)]
39. Ciez, R.E.; Whitacre, J.F. Examining different recycling processes for lithium-ion batteries. *Nat. Sustain.* **2019**, *2*, 148–156. [[CrossRef](#)]
40. Birkl, C.R.; Roberts, M.R.; McTurk, E.; Bruce, P.G.; Howey, D.A. Degradation diagnostics for lithium-ion cells. *J. Power Sources* **2017**, *341*, 373–386. [[CrossRef](#)]
41. Wang, Y.; An, N.; Wen, L.; Wang, X.; Jiang, F.; Hou, Y.; Yin, Y.; Jiang, J. Recent progress on the recycling technology of Li-ion batteries. *J. Energy Chem.* **2021**, *55*, 391–419. [[CrossRef](#)]
42. Meshram, P.; Pandey, B.D.; Mankhand, T.R. Extraction of lithium from primary and secondary sources by pre-treatment, leaching and separation: A comprehensive review. *Hydrometallurgy* **2014**, *150*, 192–208. [[CrossRef](#)]
43. Bell, A.T. The impact of nanoscience on heterogeneous catalysis. *Science* **2003**, *299*, 1688. [[CrossRef](#)]
44. Gonçalves, M.C.A.; Garcia, E.M.; Taroco, H.A.; Gorgulho, H.F.; Melo, J.O.; Silva, R.R.; Souza, A.G. Chemical recycling of cell phone Li-ion batteries: Application in environmental remediation. *Waste Manag.* **2015**, *40*, 144–150. [[CrossRef](#)] [[PubMed](#)]
45. Wang, P.; Lou, X.Y.; Chen, Q.Q.; Liu, Y.J.; Sun, X.H.; Guo, Y.G.; Zhang, X.J.; Wang, R.X.; Wang, Z.H.; Chen, S.; et al. Spent LiFePO₄: An old but vigorous peroxydisulfate activator for degradation of organic pollutants in water. *Environ. Res.* **2022**, *214*, 113780. [[CrossRef](#)] [[PubMed](#)]
46. Li, J.; Wang, G.; Xu, Z. Generation and detection of metal ions and volatile organic compounds (VOCs) emissions from the pretreatment processes for recycling spent lithium-ion batteries. *Waste Manag.* **2016**, *52*, 221–227. [[CrossRef](#)]
47. Wang, M.; Tan, Q.; Liu, L.; Li, J. A low-toxicity and high efficiency deep eutectic solvent for the separation of aluminum foil and cathode materials from spent lithium-ion batteries. *J. Hazard. Mater.* **2019**, *380*, 120846. [[CrossRef](#)]
48. Li, B.; Ma, B.; Wei, M.Y.; Li, Y.; Fan, X.B.; Zhang, F.B.; Zhang, G.L.; Xia, Q.; Peng, W.C. Synthesis of Co-NC catalysts from spent lithium-ion batteries for Fenton-like reaction: Generation of singlet oxygen with 100% selectivity. *Carbon* **2022**, *197*, 76–86. [[CrossRef](#)]
49. Xiao, J.F.; Niu, B.; Xu, Z.M. Ammonia reduction system for the diversity of cathode processing of Li-ion batteries. *ACS Sustain. Chem. Eng.* **2021**, *9*, 12091–12099. [[CrossRef](#)]
50. Dang, S.; Hou, W.; Min, Y.L.; Wu, J.F.; Xua, Q.J.; Shi, P.H. Electro-oxidation: A win-win strategy for the selective recovery of Li from spent lithium-ion batteries and the preparation of highly active catalysts. *Chem. Eng. J.* **2022**, *435*, 1335169. [[CrossRef](#)]

51. Lin, X.M.; Ma, Y.M.; Wang, Y.; Wan, J.Q.; Guan, Z.Y. Lithium iron phosphate (LiFePO₄) as an effective activator for degradation of organic dyes in water in the presence of persulfate. *RSC Adv.* **2015**, *5*, 94694. [[CrossRef](#)]
52. Garcia, E.; Teixeira, H.T. Fast electrochemical method for organic dye decolorization using recycled Li-ion batteries. *Recycling* **2018**, *3*, 35. [[CrossRef](#)]
53. Liu, Y.; Gao, W.; Zhou, H.; Yi, X.L.; Bao, Y.M. Highly reactive bulk lattice oxygen exposed by simple water treatment of LiCoO₂ for catalytic oxidation of airborne benzene. *Mol. Catal.* **2020**, *492*, 111003. [[CrossRef](#)]
54. Chen, X.; Deng, F.; Liu, X.; Cui, K.P.; Weerasooriya, R. Hydrothermal synthesis of MnO₂/Fe(0)composites from Li-ion battery cathodes for destructing sulfadiazine by photo-Fenton process. *Sci. Total. Environ.* **2021**, *774*, 145776. [[CrossRef](#)]
55. Xu, L.; Wang, J. A heterogeneous Fenton-like system with nanoparticulate zero-valent iron for removal of 4-chloro-3-methyl phenol. *J. Hazard. Mater.* **2011**, *186*, 256–264. [[CrossRef](#)]
56. Jiang, Y.W.; Gao, J.H.; Zhang, Q.; Liu, Z.Y.; Fu, M.L.; Wu, J.L.; Hu, Y.; Ye, D.Q. Enhanced oxygen vacancies to improve ethyl acetate oxidation over MnO_x-CeO₂ catalyst derived from MOF template. *Chem. Eng. J.* **2019**, *371*, 78–87. [[CrossRef](#)]
57. Li, X.T.; Ma, J.Z.; Yang, L.; He, G.Z.; Zhang, C.B.; Zhang, R.D.; He, H. Oxygen vacancies induced by transition metal doping in gamma-MnO₂ for highly efficient ozone decomposition. *Environ. Sci. Technol.* **2018**, *19*, 12685–12696. [[CrossRef](#)]
58. Li, G.; He, K.; Zhang, F.L.; Jiang, G.X.; Zhao, Z.Y.; Zhang, Z.S.; Cheng, S.; Hao, Z.P. Defect enhanced CoMnNiO_x catalysts derived from spent ternary lithium-ion batteries for low-temperature propane oxidation. *Appl. Catal. B-Environ.* **2022**, *309*, 121231. [[CrossRef](#)]
59. Dang, S.; Zhou, P.S.; Shi, P.H.; Min, Y.L.; Xu, Q.J. In situ aluminothermic reduction induced by mechanochemical activation enhances the ability of the spent LiCoO₂ cathode to activate peroxymonosulfate. *ACS Sustain. Chem. Eng.* **2021**, *9*, 15375–15385. [[CrossRef](#)]
60. Bao, Y.; Lim, T.T.; Goei, R.; Zhong, Z.; Wang, R.; Hu, X. One-step construction of heterostructured metal-organics@Bi₂O₃ with improved photo induced charge transfer and enhanced activity in photocatalytic degradation of sulfamethoxazole under solar light irradiation. *Chemosphere* **2018**, *205*, 396–403. [[CrossRef](#)]
61. Kumar, A.; Kumar, A.; Sharma, G.; Al-Muhtaseb, A.H.; Naushad, M.; Ghfar, A.A.; Stadler, F.J. Quaternary magnetic BiOCl/g-C₃N₄/Cu₂O/Fe₃O₄ nano-junction for visible light and solar powered degradation of sulfamethoxazole from aqueous environment. *Chem. Eng. J.* **2018**, *334*, 462–478. [[CrossRef](#)]
62. Kumar, A.; Kumar, A.; Sharma, G.; Naushad, M.; Ahamad, T.; Stadler, F. Utilizing recycled LiFePO₄ from batteries in combination with B@C₃N₄ and CuFe₂O₄ as sustainable nano-junctions for high performance degradation of atenolol. *Chemosphere* **2018**, *209*, 457–469. [[CrossRef](#)] [[PubMed](#)]
63. Niu, B.; Xiao, J.F.; Xu, Z.M. Utilizing spent Li-ion batteries to regulate the π-conjugated structure of g-C₃N₄: A win-win approach for waste recycling and highly active photocatalyst construction. *J. Mater. Chem. A* **2021**, *9*, 472–481. [[CrossRef](#)]
64. Dunn, J.B.; Gaines, L.; Sullivan, J.; Wang, M.Q. The impact of recycling on cradle to gate energy consumption and greenhouse gas emissions of automotive lithium-ion batteries. *Environ. Sci. Technol.* **2012**, *46*, 12704–12710. [[CrossRef](#)]
65. Zhu, S.J.; Xu, Y.P.; Zhu, Z.G.; Liu, Z.Q.; Wang, W. Activation of peroxymonosulfate by magnetic Co-Fe/SiO₂ layered catalyst derived from iron sludge for ciprofloxacin degradation. *Chem. Eng. J.* **2020**, *384*, 123298. [[CrossRef](#)]
66. Guo, H.; Min, Z.J.; Hao, Y.; Wang, X.; Fan, J.C.; Shi, P.H.; Min, Y.L.; Xu, Q.J. Sustainable recycling of LiCoO₂ cathode scrap on the basis of successive peroxymonosulfate activation and recovery of valuable metals. *Sci. Total. Environ.* **2021**, *759*, 143478. [[CrossRef](#)]
67. Zhao, Y.L.; Yuan, X.Z.; Jiang, L.B.; Li, X.D.; Zhang, J.J.; Wang, H. Reutilization of cathode material from spent batteries as a heterogeneous catalyst to remove antibiotics in wastewater via peroxymonosulfate activation. *Chem. Eng. J.* **2020**, *400*, 125903. [[CrossRef](#)]
68. Pi, Y.Q.; Gao, H.Q.; Cao, Y.D.; Cao, R.L.; Wang, Y.B.; Sun, J.H. Cobalt ferrite supported on carbon nitride matrix prepared using waste battery materials as a peroxymonosulfate activator for the degradation of levofloxacin hydrochloride. *Chem. Eng. J.* **2020**, *379*, 122377. [[CrossRef](#)]
69. Liang, J.X.; Xue, Y.X.; Gu, J.N.; Li, J.D.; Shi, F.; Guo, X.; Guo, M.M.; Min, X.; Li, K.; Sun, T.H.; et al. Sustainably recycling spent lithium-ion batteries to prepare magnetically separable cobalt ferrite for catalytic degradation of bisphenol A via peroxymonosulfate activation. *J. Hazard. Mater.* **2022**, *427*, 127910. [[CrossRef](#)]
70. Liang, J.X.; Guo, M.M.; Xue, Y.X.; Gu, J.N.; Li, J.D.; Shi, F.; Guo, X.; Min, X.; Jia, J.P.; Li, K.; et al. Constructing magnetically separable manganese-based spinel ferrite from spent ternary lithium-ion batteries for efficient degradation of bisphenol A via peroxymonosulfate activation. *Chem. Eng. J.* **2022**, *435*, 135000. [[CrossRef](#)]
71. Liu, T.; Dai, A.; Lu, J.; Yuan, Y.; Xiao, Y.; Yu, L.; Li, M.; Gim, J.; Ma, L.; Liu, J.; et al. Correlation between manganese dissolution and dynamic phase stability in spinel-based lithium-ion battery. *Nat. Commun.* **2019**, *10*, 4721. [[CrossRef](#)]
72. Wang, X.; Zhang, X.F.; Dai, L.; Guo, H.; Shi, P.H.; Min, Y.L.; Xu, Q.J. Recycling the cathode scrap of spent lithium-ion batteries as an easily recoverable peroxymonosulfate catalyst with enhanced catalytic performance. *ACS Sustain. Chem. Eng.* **2020**, *8*, 11337–11347. [[CrossRef](#)]
73. Zhang, X.; Xue, Q.; Li, L.; Fan, E.; Wu, F.; Chen, R. Sustainable recycling and regeneration of cathode scraps from industrial production of lithium-ion batteries. *ACS Sustain. Chem. Eng.* **2016**, *4*, 7041–7049. [[CrossRef](#)]

74. Zhao, Y.L.; Wang, H.; Ji, J.Q.; Li, X.D.; Yuan, X.Z.; Duan, A.; Guar, X.; Jiang, L.; Li, Y. Recycling of waste power lithium-ion batteries to prepare nickel/cobalt/manganese-containing catalysts with inter-valence cobalt/manganese synergistic effect for peroxymonosulfate activation. *J. Colloid Interf. Sci.* **2022**, *626*, 562–580. [[CrossRef](#)] [[PubMed](#)]
75. Zhao, Y.L.; Wang, H.; Ji, J.Q.; Li, X.D.; Yuan, X.Z.; Jiang, L.B.; Yang, J.J.; Shao, Y.N.; Guan, X. Degradation of ciprofloxacin by peroxymonosulfate activation using catalyst derived from spent lithium-ion batteries. *J. Clean. Prod.* **2022**, *362*, 132442. [[CrossRef](#)]
76. Palacín, M.R. Understanding ageing in Li-ion batteries: A chemical issue. *Chem. Soc. Rev.* **2018**, *47*, 4924–4933. [[CrossRef](#)]
77. Peng, D.Z.; Zhang, J.F.; Zou, J.T.; Ji, G.J.; Ye, L.; Li, D.M.; Zhang, B. Closed-loop regeneration of LiFePO₄ from spent lithium-ion batteries: A “feed three birds with one scone” strategy toward advanced cathode materials. *J. Clean. Prod.* **2021**, *316*, 128098. [[CrossRef](#)]
78. Chen, L.; Peng, X.; Liu, J.; Li, J.; Wu, F. Decolorization of Orange I in aqueous solution by an Fe(II)/sulfite system: Replacement of persulfate. *Ind. Eng. Chem. Res.* **2012**, *51*, 13632–13638. [[CrossRef](#)]
79. Jiang, B.; Liu, Y.; Zheng, J.; Tan, M.; Wang, Z.; Wu, M. Synergetic transformations of multiple pollutants driven by Cr(VI)-sulfite reactions. *Environ. Sci. Technol.* **2015**, *49*, 12363–12371. [[CrossRef](#)]
80. Sun, B.; Bao, Q.; Guan, X. Critical role of oxygen for rapid degradation of organic contaminants in permanganate/bisulfite process. *J. Hazard. Mater.* **2018**, *352*, 157–164. [[CrossRef](#)]
81. Shi, Z.; Jin, C.; Zhang, J.; Zhu, L. Insight into mechanism of arsenic acid degradation in permanganate sulfite system: Role of reactive species. *Chem. Eng. J.* **2019**, *359*, 1463–1471. [[CrossRef](#)]
82. Dong, H.; Wei, G.; Cao, T.; Shao, B.; Guan, X.; Strathmann, T.J. Insights into the oxidation of organic contaminants during Cr(VI) reduction by sulfite: The overlooked significance of Cr(V). *Environ. Sci. Technol.* **2020**, *54*, 1157–1166. [[CrossRef](#)] [[PubMed](#)]
83. Guo, Y.; Lou, X.; Fang, C.; Xiao, D.; Wang, Z.; Liu, J. Novel photo-sulfite system: Toward simultaneous transformations of inorganic and organic pollutants. *Environ. Sci. Technol.* **2013**, *47*, 11174–11181. [[CrossRef](#)] [[PubMed](#)]
84. Lee, Y.J.; Rochelle, G.T. Oxidative degradation of organic acid conjugated with sulfite oxidation in flue gas desulfurization: Products, kinetics and mechanism. *Environ. Sci. Technol.* **1987**, *21*, 266–272. [[CrossRef](#)]
85. Brandt, C.; Fábian, I.; van Eldik, R. Kinetics and mechanism of the iron(III)-catalyzed autoxidation of sulfur(IV) oxides in aqueous solution. Evidence for the redox cycling of iron in the presence of oxygen and modeling of the overall reaction mechanism. *Inorg. Chem.* **1994**, *33*, 687–701. [[CrossRef](#)]
86. Guo, Y.G.; Zhao, Y.L.; Lou, X.Y.; Zhou, T.Y.; Wang, Z.H.; Fang, C.L.; Guan, J.; Chen, S.; Xu, X.; Zhang, R.Q. Efficient degradation of industrial pollutants with sulfur(IV) mediated by LiCoO₂ cathode powders of spent lithium ion batteries: A “treating waste with waste” strategy. *J. Hazard. Mater.* **2020**, *390*, 123090. [[CrossRef](#)]
87. Prasad, D.S.N.; Rani, A.; Gupta, K.S. Surface-catalyzed autoxidation of sulfur(IV) in aqueous silica and copper(II) oxide suspensions. *Environ. Sci. Technol.* **1992**, *26*, 1361–1368. [[CrossRef](#)]
88. Brandt, C.; Eldik, M. Transition metal-catalyzed oxidation of sulfur(IV) oxides atmospheric-relevant processes and mechanisms. *Chem. Rev.* **1995**, *93*, 119–190. [[CrossRef](#)]
89. Huang, Y.F.; Huang, Y.Y.; Chiueh, P.T.; Lo, S.L. Heterogeneous Fenton oxidation of trichloroethylene catalyzed by sewage sludge biochar: Experimental study and life cycle assessment. *Chemosphere* **2020**, *249*, 126139. [[CrossRef](#)]
90. Lyu, L.; Yu, G.F.; Zhang, L.L.; Hu, C.; Sun, Y. 4-phenoxyphenol-functionalized reduced graphene oxide nanosheets: A metal-free Fenton-like catalyst for pollutant destruction. *Environ. Sci. Technol.* **2018**, *52*, 747–756. [[CrossRef](#)]
91. Zou, W.S.; Li, J.; Wang, R.H.; Ma, J.Y.; Chen, Z.J.; Duan, L.L.; Mi, H.W.; Chen, H. Hydroxylamine mediated Fenton-like interfacial reaction dynamics on sea urchin-like catalyst derived from spent LiFePO₄ battery. *J. Hazard. Mater.* **2022**, *431*, 128590. [[CrossRef](#)] [[PubMed](#)]
92. Zhang, Y.; Chen, Z.; Zhou, L.; Wu, P.; Zhao, Y.; Lai, Y.; Wang, F. Heterogeneous Fenton degradation of bisphenol A using Fe₃O₄@beta-CD/rGO composite: Synergistic effect, principle and way of degradation. *Environ. Pollut.* **2019**, *244*, 93–101. [[CrossRef](#)] [[PubMed](#)]
93. Zhou, H.; Peng, J.; Li, J.; You, J.; Lai, L.; Liu, R.; Ao, Z.; Ya, G.; La, B. Metal-free black-red phosphorus as an efficient heterogeneous reductant to boost Fe⁺/Fe²⁺ cycle for peroxymonosulfate activation. *Water Res.* **2021**, *188*, 116529. [[CrossRef](#)] [[PubMed](#)]
94. Zhu, Y.; Zhu, R.; Xi, Y.; Zhu, J.; Zhu, G.; He, H. Strategies for enhancing the Heterogeneous Fenton catalytic reactivity: A review. *Appl. Catal. B Environ.* **2019**, *255*, 117739. [[CrossRef](#)]
95. Zhu, Y.; Zhu, R.; Yan, L.; Fu, H.; Xi, Y.; Zhou, H.; Zhu, G.; Zhu, J.; He, H. Visible-light Ag/AgBr/ferrihydrite catalyst with enhanced heterogeneous photo-Fenton reactivity via electron transfer from Ag/AgBr to ferrihydrite. *Appl. Catal. B Environ.* **2018**, *239*, 280–289. [[CrossRef](#)]
96. Yan, Q.; Lian, C.; Huang, K.; Liang, L.; Xing, M. Constructing an acidic microenvironment by MoS₂ in heterogeneous Fenton reaction for pollutant control. *Angew. Chem.* **2021**, *60*, 2–11. [[CrossRef](#)]
97. Guan, J.; Li, Z.X.; Chen, X.; Gu, W.X. Zero-valent iron supported on expanded graphite from spent lithium-ion battery anodes and ferric chloride for the degradation of 4-chlorophenol in water. *Chemosphere* **2022**, *290*, 133381. [[CrossRef](#)]
98. Zhang, M.H.; Dong, H.; Zhao, L.; Wang, D.X.; Meng, D. A review on Fenton process for organic wastewater treatment based on optimization perspective. *Sci. Total Environ.* **2019**, *670*, 110–121. [[CrossRef](#)]
99. Bedia, J.; Bolver, C.; Ponce, S.; Rodriguez, J.; Rodriguez, J.J. Adsorption of antipyrine by activated carbons from FeCl₃ activation of tara gum. *Chem. Eng. J.* **2018**, *333*, 58–65. [[CrossRef](#)]
100. Mishra, S.; Bal, R.; Dey, R.K. Heterogeneous recyclable copper oxide supported on activated red mud as an efficient and stable catalyst for the one pot hydroxylation of benzene to phenol. *Mol. Catal.* **2021**, *499*, 111310. [[CrossRef](#)]

101. Vega, G.; Quintanilla, A.; Belmonte, M.; Casas, J.A. Kinetic study of phenol hydroxylation by H₂O₂ in 3D Fe/SiC honeycomb monolithic reactors: Enabling the sustainable production of dihydroxy benzenes. *Chem. Eng. J.* **2022**, *428*, 131128. [[CrossRef](#)]
102. Guo, M.M.; Li, K.; Liu, L.Z.; Zhang, H.B.; Guo, W.M.; Hu, X.F.; Min, X.; Jia, J.P.; Sun, T.H. Manganese-based multi-oxide derived from spent ternary lithium-ions batteries as high-efficient catalyst for VOCs oxidation. *J. Hazard. Mater.* **2019**, *380*, 120905. [[CrossRef](#)] [[PubMed](#)]
103. Guo, M.M.; Liu, L.Z.; Gu, J.N.; Zhang, H.B.; Min, X.; Liang, J.X.; Jia, J.P.; Li, K.; Sun, T.H. Improved performance of volatile organic compounds oxidation over MnO_x and GdMnO₃ composite oxides from spent lithium-ion batteries: Effect of acid treatment. *Chin. J. Chem. Eng.* **2021**, *34*, 278–288. [[CrossRef](#)]
104. Sun, J.T.; Liu, L.Z.; Zhang, Y.; Guo, M.M.; Zhou, B. Improved catalytic oxidation of propylene glycol methyl ether over Sm-Mn and Sm-Co perovskite-based catalysts prepared by the recycling of spent ternary lithium-ion battery. *Environ. Sci. Pollut. R.* **2021**, *28*, 38829–38838. [[CrossRef](#)]
105. Sun, J.T.; Min, X.; Gu, J.N.; Liang, J.X.; Guo, M.M. Improved performance of Mn-, Co-based oxides from spent lithium-ion batteries supported on CeO₂ with different morphol Recovery of cathode materialsogies for 2-ethoxyethyl acetate oxidation. *J. Environ. Chem. Eng.* **2021**, *9*, 104964. [[CrossRef](#)]
106. Guo, M.M.; Li, K.; Zhang, H.B.; Min, X.; Liang, J.X.; Hu, X.F.; Guo, W.M.; Jia, J.P.; Sun, T.H. Promotional removal of oxygenated VOC over manganese-based multi oxides from spent lithium-ions manganese batteries: Modification with Fe, Bi and Ce dopants. *Sci. Total Environ.* **2020**, *740*, 139951. [[CrossRef](#)]
107. Guo, M.M.; Wang, X.N.; Liu, L.Z.; Min, X.; Hu, X.F.; Guo, W.M.; Zhu, N.W.; Jia, J.P.; Sun, T.H.; Li, K. Recovery of cathode materials from spent lithium-ion batteries and their application in preparing multi-metal oxides for the removal of oxygenated VOCs: Effect of synthetic methods. *Environ. Res.* **2021**, *193*, 110563. [[CrossRef](#)]
108. Wang, L.; Li, Y.; Liu, J.; Tian, Z.; Jing, Y. Regulation of oxygen vacancies in vobalt-cerium oxide catalyst for boosting decontamination of VOCs by catalytic oxidation. *Sep. Purif. Technol.* **2021**, *277*, 119505. [[CrossRef](#)]
109. Guo, J.; Zhang, J.; Chen, C.; Lan, Y.Q. Rapid photodegradation of methyl orange by oxalic acid assisted with cathode material of lithium ion batteries LiFePO₄. *J. Taiwan Inst. Chem. E* **2016**, *62*, 187–191. [[CrossRef](#)]
110. Ong, W.J.; Tan, L.L.; Ng, Y.H.; Yong, S.T.; Chai, S.P. Graphitic carbon nitride (g-C₃N₄)-based photocatalysts for artificial photosynthesis and environmental remediation: Are we a step closer to achieving sustainability? *Chem. Rev.* **2016**, *116*, 7159–7329. [[CrossRef](#)] [[PubMed](#)]
111. Zhang, J.; Chen, Y.; Wang, X. Two-dimensional covalent carbon nitride nanosheets: Synthesis, functionalization, and applications. *Energy Environ. Sci.* **2015**, *8*, 3092–3108. [[CrossRef](#)]
112. Niu, B.; Xiao, J.F.; Xu, Z.M. Recycling spent LiCoO₂ battery as a high-efficient lithium doped graphitic carbon nitride/Co₃O₄ composite photocatalyst and its synergistic photocatalytic mechanism. *Energy Environ. Mater.* **2022**. [[CrossRef](#)]
113. Huang, H.; Xu, Y.; Feng, Q.; Leung, D.Y.C. Low temperature catalytic oxidation of volatile organic compounds: A review. *Catal. Sci. Technol.* **2015**, *5*, 2649–2669. [[CrossRef](#)]
114. Hu, X.; Yu, Y.; Chen, D.; Xu, W.; Fang, J.; Liu, Z.; Li, R.; Yao, L.; Qin, J.; Fang, Z. Anatase/rutile homojunction quantum dots anchored on g-C₃N₄ nanosheets for antibiotics degradation in seawater matrixe via coupled adsorption-photocatalysis: Mechanism insight and toxicity evaluation. *Chem. Eng. J.* **2022**, *432*, 134375. [[CrossRef](#)]
115. Landi, S.; Segundo, I.R.; Freitas, E.; Vasilevskiy, M.; Carneiro, J.; Tavares, C.J. Use and misuse of the Kubelka-Munk function to obtain the band gap energy from diffuse reflectance measurements. *Solid State Commun.* **2022**, *341*, 114573. [[CrossRef](#)]
116. Rumana, H.; Veena, S. Microrecycled Co₃O₄ from waste lithium-ion battery: Synthesis, characterization and implication in environmental application. *J. Environ. Chem. Eng.* **2022**, *10*, 107858. [[CrossRef](#)]
117. Friedmann, D.; Mendive, C.; Bahnmann, D. TiO₂ for water treatment: Parameters affecting the kinetics and mechanisms of photocatalysis. *Appl. Catal. B* **2010**, *99*, 398–406. [[CrossRef](#)]
118. Zhu, S.J.; Wang, W.; Xu, Y.P.; Zhu, Z.G.; Liu, Z.Q.; Cu, F.Y. Iron sludge-derived magnetic Fe⁰/Fe₃C catalyst for oxidation of ciprofloxacin via peroxymonosulfate activation. *Chem. Eng. J.* **2019**, *365*, 99–110. [[CrossRef](#)]
119. Wu, Y.T.; Cai, T.; Chen, X.J.; Duan, X.D.; Xu, G.G.; Bu, L.J.; Zhou, S.Q.; Shi, Z. Unveiling the interaction of epigallocatechin-3-gallate with peroxymonosulfate for degradation of bisphenol S: Two-stage kinetics and identification of reactive species. *Sep. Purif. Technol.* **2021**, *274*, 119040. [[CrossRef](#)]
120. Hong, Y.C.; Zhou, H.Y.; Xiong, Z.K.; Liu, Y.; Yao, G.; Lai, B. Heterogeneous activation of peroxymonosulfate by CoMgFe-LDO for degradation of carbamazepine: Efficiency, mechanism and degradation pathways. *Chem. Eng. J.* **2020**, *391*, 123604. [[CrossRef](#)]
121. Chen, X.X.; Fu, L.Y.; Yu, Y.; Wu, C.Y.; Li, M.; Jin, X.G.; Yang, J.; Wang, P.X.; Chen, Y. Recent development in sludge biochar-based catalysts for advanced oxidation processes of wastewater. *Catalysts* **2021**, *11*, 1275. [[CrossRef](#)]
122. Xiao, J.D.; Xie, Y.B.; Cao, H.B. Organic pollutants removal in wastewater by heterogeneous photocatalytic ozonation. *Chemosphere* **2015**, *121*, 1–17. [[CrossRef](#)]
123. Weng, X.; Sun, P.; Long, Y.; Meng, Q.; Wu, Z. Catalytic oxidation of chlorobenzene over Mn_xCe_{1-x}O₂/HZSM-5 catalysts: A study with practical implications. *Environ. Sci. Technol.* **2017**, *51*, 8057–8066. [[CrossRef](#)] [[PubMed](#)]
124. Yu, Y.; Huang, F.; He, Y.; Liu, X.Y.; Song, C.J.; Xu, Y.H.; Zhang, Y.J. Heterogeneous Fenton-like degradation of ofloxacin over sludge derived carbon as catalysts: Mechanism and performance. *Sci. Total Environ.* **2019**, *654*, 942–947. [[CrossRef](#)]

125. Guo, M.M.; Li, K.; Liu, L.Z.; Zhang, H.B.; Guo, W.M.; Hu, X.F.; Min, X.; Jia, J.P.; Sun, T.H. Insight into a sustainable application of spent lithium-ion cobaltate batteries: Preparation of a cobalt-based oxide catalyst and its catalytic performance in toluene oxidation. *Ind. Eng. Chem. Res.* **2020**, *59*, 194–204. [[CrossRef](#)]
126. Dai, T.C.; Zhou, H.; Liu, Y.; Cao, R.R.; Zhan, J.J.; Liu, L.F.; Jang, W.L. Synergy of lithium, cobalt, and oxygen vacancies in lithium cobalt oxide for airborne benzene oxidation: A concept of reusing electronic wastes for air pollutant removal. *ACS Sustain. Chem. Eng.* **2019**, *7*, 5072–5081. [[CrossRef](#)]
127. Liu, Y.; Gao, W.; Zhan, J.J.; Bao, Y.M.; Cao, R.R.; Zhou, H.; Liu, L.F. One-pot synthesis of Ag-H₃PW₁₂O₄₀-LiCoO₂ composites for thermal oxidation of airborne benzene. *Chem. Eng. J.* **2019**, *375*, 121956. [[CrossRef](#)]
128. Chan, K.H.; Chu, W. Degradation of atrazine by cobalt-mediated activation of peroxydisulfate: Different cobalt counter anions in homogenous process and cobalt oxide catalysts in photolytic heterogeneous process. *Water Res.* **2009**, *43*, 2513–2521. [[CrossRef](#)]
129. Lyu, J.; Ge, M.; Hu, Z.; Guo, C. One-pot synthesis of magnetic CuO/Fe₂O₃/CuFe₂O₄ nanocomposite to activate persulfate for levofloxacin removal: Investigation of efficiency, mechanism and degradation route. *Chem. Eng. J.* **2020**, *389*, 124456. [[CrossRef](#)]
130. Devi, P.; Das, U.; Dalai, A.K. In-situ chemical oxidation: Principle and applications of peroxide and persulfate treatments in waste water systems. *Sci. Total. Environ.* **2016**, *571*, 643–657. [[CrossRef](#)]
131. Wu, Z.; Wang, Y.; Xiong, Z.; Ao, Z.; Pu, S.; Yao, G.; Lai, B. Core-shell magnetic Fe₃O₄@Zn/Co-ZIFs to activate peroxydisulfate for highly efficient degradation of carbamazepine. *Appl. Catal. B Environ.* **2020**, *277*, 119136. [[CrossRef](#)]
132. Zhu, M.P.; Yang, J.C.E.; Delai Sun, D.; Yuan, B.; Fu, M.L. Deciphering the simultaneous removal of carbamazepine and metronidazole by monolithic Co₂AlO₄@Al₂O₃ activated peroxydisulfate. *Chem. Eng. J.* **2022**, *436*, 135201. [[CrossRef](#)]
133. Dong, X.; Ren, B.; Sun, Z.; Li, C.; Zhang, X.; Kong, M.; Zheng, S.; Dionysiou, D.D. Monodispersed CuFe₂O₄ nanoparticles anchored on natural kaolinite as highly efficient peroxydisulfate catalyst for bisphenol A degradation. *Appl. Catal. B* **2019**, *253*, 206–217. [[CrossRef](#)]
134. Cai, C.; Kang, S.; Xie, X.; Liao, C.; Duan, X.; Dionysiou, D.D. Efficient degradation of bisphenol A in water by heterogeneous activation of peroxydisulfate using highly active cobalt ferrite nanoparticles. *J. Hazard. Mater.* **2020**, *399*, 122979. [[CrossRef](#)]
135. Lin, H.; Li, S.; Deng, B.; Tan, W.; Li, R.; Xu, Y.; Zhang, H. Degradation of bisphenol A by activating peroxydisulfate with Mn_{0.6}Zn_{0.4}Fe₂O₄ fabricated from spent Zn-Mn alkaline batteries. *Chem. Eng. J.* **2019**, *364*, 541–551. [[CrossRef](#)]
136. Xue, Y.; Wang, Z.; Naidu, R.; Bush, R.; Yang, F.; Liu, J.; Huang, M. Role of halide ions on organic pollutants degradation by peroxygens-based advanced oxidation processes: A critical review. *Chem. Eng. J.* **2022**, *433*, 134546. [[CrossRef](#)]
137. Dan, J.; Rao, P.; Wang, Q.; Dong, L.; Chen, J. MgO-supported CuO with encapsulated structure for enhanced peroxydisulfate activation to remove thiamphenicol. *Sep. Purif. Technol.* **2021**, *280*, 119782. [[CrossRef](#)]

Disclaimer/Publisher's Note: The statements, opinions and data contained in all publications are solely those of the individual author(s) and contributor(s) and not of MDPI and/or the editor(s). MDPI and/or the editor(s) disclaim responsibility for any injury to people or property resulting from any ideas, methods, instructions or products referred to in the content.